R. & M. No. 3355

MINISTRY OF AVIATION

AERONAUTICAL RESEARCH COUNCIL
REPORTS AND MEMORANDA

Oscillatory-Derivative Measurements on Sting-Mounted Wind-Tunnel Models: Method of Test and Results for Pitch and Yaw on a Cambered Ogee Wing at Mach Numbers up to 2·6

By J. S. Thompson, B.A. and R. A. Fail, B.Sc.

LONDON: HER MAJESTY'S STATIONERY OFFICE
1964
PRICE £1 1s. 0d. NET

Oscillatory-Derivative Measurements on Sting-Mounted Wind-Tunnel Models: Method of Test and Results for Pitch and Yaw on a Cambered Ogee Wing at Mach Numbers up to 2·6

By J. S. THOMPSON, B.A. and R. A. FAIL, B.Sc.

COMMUNICATED BY THE DEPUTY CONTROLLER AIRCRAFT (RESEARCH AND DEVELOPMENT), MINISTRY OF AVIATION

*Reports and Memoranda No. 3355**

July, 1962

Summary.

This report describes a method which has been developed for measuring oscillatory derivatives on sting-mounted models in the 8 ft by 8 ft Supersonic Tunnel at R.A.E. Bedford. Direct and cross derivatives with respect to angular displacements and velocities in pitch and yaw have been measured satisfactorily, and results are given of tests on a cambered ogee wing at six Mach numbers from 0·2 to 2·6. Some tests were made on this model in the course of the preliminary development work in the 13 ft by 9 ft Low-Speed Wind Tunnel, and results of these are included.

LIST OF CONTENTS

* Replaces R.A.E. Report No. Aero. 2668—A.R.C. 24 149.

LIST OF APPENDICES

LIST OF TABLES

LIST OF ILLUSTRATIONS

---

1. *Introduction.*

Equipment has been developed for measuring oscillatory derivatives on sting-mounted models in the 8 ft Supersonic Wind Tunnel at the Royal Aircraft Establishment, Bedford. The main object has been to measure stability derivatives and cross derivatives due to angular velocity in pitch, roll, and yaw. Derivatives with respect to angular displacement can also be measured, but these are not expected to differ significantly from the static values obtained from conventional tunnel tests. It is also possible to obtain derivatives for motion in vertical or horizontal translation (heave or sideslip), but the apparatus was not designed for this purpose, and no great accuracy can be obtained.

There are some new features in the design of this equipment, since none of the published methods seemed entirely suitable for these tests. Bratt[1] has given a survey of existing techniques: many of them are applicable only to low-speed tests, others are for high-speed two-dimensional or half-model tests. Beam[2] has developed a method for sting-mounted models, but it is apparently only suitable for a model with a fairly large fuselage to accommodate the internal spring unit, and of special light-weight construction. The equipment described in this report can be used for testing slender wings of conventional fibreglass construction, and a technique has been developed for allowing for the effects of the flexibility of the sting.

The present report deals with pitching and yawing tests. The apparatus for rolling tests has been made but has not yet been used.

Section 3 of this report gives a general description of the method of test and Section 4, which forms the bulk of the report, describes the equipment and the technique of testing, analysis and calibration. In Section 5 an assessment is made of the usefulness and reliability of the method, some reference being made to the results of aerodynamic tests on a cambered ogee wing which are fully described in Section 6. Section 7 mentions future work to be done.

In the four Appendices further details of the equipment and technique are given, for the benefit of other workers in the same field who may be interested.

2. *Notation.*

Axes. All forces, moments, displacements, derivatives, and coefficients are referred to a system of earth axes fixed in the mean position of the oscillating model, called 'sting axes' in this report.

Certain other axes mentioned in the report are defined in Appendix III Section 1.

Displacements, Velocities, and Accelerations (Assumed Small).

x	$\dot{x}$	$\ddot{x}$	forwards
y	$\dot{y}$	$\ddot{y}$	sideslip
z	$\dot{z}$	$\ddot{z}$	heave
ϕ	$\dot{\phi}$	$\ddot{\phi}$	roll
θ	$\dot{\theta}$	$\ddot{\theta}$	pitch
ψ	$\dot{\psi}$	$\ddot{\psi}$	yaw.

Model Inertias.

W	Mass
$\bar{x}\ \bar{y}\ \bar{z}$	Co-ordinates of c.g.
$I_{xx}\ I_{yy}\ I_{zz}$	Moments of inertia
$I_{yz}\ I_{zx}\ I_{xy}$	Products of inertia.

Forces and Moments.

Side force	$Y = \frac{1}{2}\rho V^2 S C_Y$
Normal force	$Z = \frac{1}{2}\rho V^2 S C_Z$
Rolling moment	$L = \frac{1}{2}\rho V^2 S b C_l$
Pitching moment	$M = \frac{1}{2}\rho V^2 S C_0 C_m$
Yawing moment	$N = \frac{1}{2}\rho V^2 S b C_n$.

Derivatives are denoted by suffixes, e.g.

$M_\theta = \partial M/\partial\theta$ = pitching moment due to pitch displacement.

These symbols are used for the derivatives as measured, i.e. the sum of the mechanical and aerodynamic components.

Non-dimensional aerodynamic derivatives, denoted by small letters (e.g. m_θ) are obtained by multiplying the aerodynamic component of the derivative by two factors, one depending on the type of force or moment, the other on the type of motion or displacement. These factors are as follows:

Force or moment	Factor
M	$1/\rho V^2 S C_0$
N or L	$1/\rho V^2 S(\frac{1}{2}b)$
Z or Y	$1/\rho V^2 S$

Motion or displacement	Factor
θ, ϕ, or ψ	1
$\dot{\theta}$	V/C_0
$\dot{\phi}$ or $\dot{\psi}$	$V/(\frac{1}{2}b)$
y	$(\frac{1}{2}b)$
z	C_0
$\dot{y}$ or $\dot{z}$	V
$\ddot{y}$	$V^2/(\frac{1}{2}b)$
$\ddot{z}$	V^2/C_0

Thus, for instance,

$$m_{\dot{\theta}} = M_{\dot{\theta}}(1/\rho V^2 S C_0)(V/C_0) = M_{\dot{\theta}}/\rho V S C_0^2 .$$

The derivatives have been expressed in this form because that is how they were measured, and there was not generally enough information to convert them to the more usual aerodynamic forms. Complete conversion equations are given in Appendix IV.

The following relations hold between the derivatives as measured, and for comparisons at small incidences they may be simplified by putting $\cos\alpha = 1$ and omitting terms in $\sin\alpha$.

Longitudinal.

$$m_\theta = m_{\dot{z}} \cos\alpha - m_{\dot{x}} \sin\alpha \qquad (= \tfrac{1}{2}\partial C_m/\partial\alpha \text{ if } \nu = 0)$$

$$z_\theta = z_{\dot{z}} \cos\alpha - z_{\dot{x}} \sin \qquad \alpha (= \tfrac{1}{2}\partial C_z/\partial\alpha \text{ if } \nu = 0).$$

Lateral ($\beta = 0$).

$$n_\psi = -n_{\dot{y}} \cos \qquad \alpha (= -\partial C_n/\partial\beta \text{ if } \nu = 0)$$

$$l_\psi = -l_{\dot{y}} \cos \qquad \alpha (= -\partial C_l/\partial\beta \text{ if } \nu = 0)$$

$$y_\psi = -y_{\dot{y}} \cos \qquad \alpha (= -\partial C_y/\partial\beta \text{ if } \nu = 0).$$

Other Symbols.

a	(Usually suffix) pitching or yawing mode
b	(Usually suffix) heaving or sideslipping mode
b	Wing span
C_0	Wing centre-line chord
e	(Suffix) excitation force or moment
F, F'	Exciting force
h	Distance of calibrating-frame axis forward of reference axis
I_1, I_2	Generalised inertias
i	(Suffix) imaginary (quadrature) component of vector
K	Damping
K_1, K_2	Generalised damping
k	Transducer calibration factor
M	Mach number (used occasionally where no confusion arises with pitching moment)
n	Number of increments
Q	Generalised excitation
r	(Suffix) real (in-phase) component of vector
S	Wing area
$u = 1/\omega^2$	
$u_1 = -I_{yy}/M_\theta$	
$u_2 = -W/Z_z$	

Other Symbols—continued.

V	Wind velocity
v	Voltage ratio
α	Angle of incidence (datum is sting axis, *see* Fig. 6)
β	Angle of sideslip
ϵ	Phase angle
η, ξ	Generalised displacements
λ	Stiffness
λ_1, λ_2	Generalised stiffnesses
ν	Frequency parameter $\omega C_0/V$ longitudinal $\omega b/2V$ lateral
ρ	Air density
ω	Frequency (radians/second)
ω_0	Resonance frequency
ω_1, ω_2	Frequencies near resonance
ω_3	Natural frequency of roll oscillation.

3. *General Principles of Tests.*

There are many possible methods of measuring aerodynamic derivatives, but the special requirements of these tests on sting-mounted models restrict the choice considerably. To measure cross derivatives, it is necessary to provide continuous excitation, and in order to keep the excitation forces down to a reasonable value, the inertia forces must be balanced by springs; in other words, tests must be made at or near the resonant frequency of the system. A compact and easily controlled form of excitation is required, provided in the present case by an electromagnetic vibration generator.

For measuring pitching derivatives, a pitching flexure is provided in the attachment of the model to the sting, with a control spring to give a suitable natural frequency. Pitching oscillations are then excited at constant amplitude, first with wind off, then with wind on, and the frequency and the exciting couple are measured. The flexibility of the sting will allow some vertical movement of the axis: this is also measured.

In the ideal case, if this vertical movement were very small, we could then obtain the aerodynamic pitching derivatives as follows:

Stiffness M_θ from the change in natural frequency

Damping $M_{\dot\theta}$ from the change in the excitation couple

Cross stiffness Z_θ, Cross damping $Z_{\dot\theta}$ } from the changes in the in-phase and quadrature components of the vertical movement.

In practice, however, the changes in the amount of vertical movement cause appreciable displacements of the oscillation axis. To allow for this we have to know the heaving derivatives

M_z $M_{\dot{z}}$ Z_z $Z_{\dot{z}}$. These are measured by exciting a vertical oscillation (which will be accompanied by some angular movement), and measuring the changes in natural frequency, excitation force, and angular movement. These in turn require corrections for the angular movement, for which the values of pitching derivatives are needed.

The analysis is simplified by treating the system from the start as having two degrees of freedom, with two natural modes of vibration, one predominantly pitching, the other predominantly heaving. Although these can thus be described as two-degree-of-freedom tests, the primary object is to measure the pitching derivatives: the heaving derivatives appear as a by-product in the course of the analysis.

Yawing derivatives are measured in the same way, with sideslip derivatives appearing as a by-product. The rolling-moment derivatives L_ψ and $L_{\dot{\psi}}$ are measured in a straightforward way by means of a balance, or the equivalent, and L_y and $L_{\dot{y}}$ can also be obtained.

This method is in some respects a development of the well-known technique of measuring pitching derivatives for two positions of the oscillation axis. There is, however, one important distinction. The positions of these axes are considerably affected by the aerodynamic conditions. (A typical example is shown in Fig. 7.) These variations are measured and allowed for in the method here described, whereas previously they have usually been neglected, perhaps without sufficient justification.

4. *Method of Test.*

4.1. *Equipment.*

This section gives a general description of the equipment used in the test, under three headings: mechanical arrangement, excitation and control, and measurements. Further details of the various components are given in Appendix I.

4.1.1. *Mechanical arrangement.*—The use of the various parts of the equipment is shown in Fig. 1, which gives diagrammatically the arrangements for exciting and measuring combined yaw-sideslip oscillations.

The model is mounted on the end of a sting by means of a pivot allowing rotation about a vertical axis. In practice a crossed-spring flexure (described below) is used to provide both the pivot and the spring control shown on the diagram. This spring centre is located near the centre of pressure of the wing, in order to avoid large deflections under steady aerodynamic loads, particularly when the model is mounted for pitching-oscillation tests. The motion of the model consists of a yawing component produced partly by rotation of the model about this pivot and partly by bending of the end of the sting, and a sideslip component produced by the lateral deflection of the end of the sting.

These two components are present in different proportions in the two natural modes of the system. The yawing mode includes a certain amount of sideslip motion of the spring centre, while the sideslip mode includes an appreciable amount of yawing motion, and similarly for pitch and heave.

The yawing natural frequency is determined by the stiffness of the spring unit, which has been designed to give a suitable frequency parameter in the high-speed tests. The design of the sting, however, is fixed by considerations of strength and deflection under static loads, and there is not much freedom of choice in the sideslip natural frequency.

The driving force is provided by an exciter coupled to a driving rod passing through a hole inside the sting, with a linkage at the model end to convert the longitudinal force in the rod into a couple

acting between the end of the sting and the model. (Here again all pivots are formed by spring links, and the only intermediate support for the driving rod is a practically frictionless P.T.F.E. bush.) This couple can be used to excite either mode at will, simply by using the appropriate frequency, which in the tests described was about 6 c/s in the yawing mode and about 18 c/s for the predominantly sideslip mode.

It is not, perhaps, immediately obvious how an internal exciting couple acting between the model and the end of the sting can produce lateral oscillations, when a similar static couple could produce no lateral deflection. The reason is that in the natural mode of oscillation in sideslip there is a certain amount of relative angular movement between the model and the end of the sting (even when there is no yawing component in the oscillation). It is thus possible for the excitation couple to feed energy into the system in this mode.

The spring unit for pitch or yaw oscillations is shown in Fig. 2. It consists of a crossed-spring centre with unequal arms: a vertical (or lateral) member in the form of a thin flat strip, and a pair of longitudinal members which also provide the necessary spring constraint. The forward cylindrical part of the unit fits into a housing inside the model, with provision for attachment at two roll positions at 90°, and the rear end is attached to the forward end of the sting by the standard taper fitting used for 8 ft Tunnel models (not shown in the sketch). Mountings are provided for three accelerometers in the positions shown. The electrical connections from these are brought out through the hollow driving rod.

4.1.2. *Excitation and control.*—The oscillations are controlled by adjusting the frequency and output of a variable-frequency oscillator which feeds the exciter through a power amplifier, as shown in Fig. 1. It is not essential that the frequency should be exactly at resonance, as long as the phase angle between the displacement and the exciting force can be accurately measured. In practice it is usually easier to make this angle exactly 90° (corresponding to 'phase resonance') than to measure it with the required precision.

A ballast resistance between the power amplifier and the exciter (Fig. 3) reduces the effects of changes in the effective exciter impedance near resonance.

There is no difficulty in setting the oscillator to give the required vibration conditions, and maintaining these steady in tests with or without wind on.

For testing in conditions where the aerodynamic damping is negative, a feedback amplifier is used to provide artificial positive damping. This amplifier receives a signal from a pick-up on the model, shifts its phase by 90°, amplifies it as required, and adds it to the output of the variable-frequency oscillator supplying the power amplifier. This arrangement makes the total damping positive, so that the oscillations can be controlled by the variable-frequency oscillator in the usual way. The artificial damping is not included in the measurements: when the negative aerodynamic damping exceeds the positive structural damping in the system, the exciting force is recorded as negative.

The feedback damping can work quite independently of the normal excitation system, although they share the same power amplifier and exciter. In one test an unwanted yawing oscillation at 6 c/s was effectively damped out while a sideslip oscillation at 18 c/s was being excited and measured.

As a safety precaution, it is arranged that a trip contact is made when the oscillation amplitude reaches a certain value, and this immediately switches off the oscillator output and applies maximum damping from the feedback amplifier.

4.1.3. *Measurements.*—The oscillator frequency is measured by an electronic counter which measures the time for one cycle (or ten cycles) in microseconds.

The excitation force or couple is measured in terms of the exciter current, or rather as the voltage across a fixed resistance in the supply lead to the exciter. The method of calibration is described below.

The remaining three measurements could be obtained as balance measurements, i.e. as measurements of strains or relative displacements, but for most applications there are advantages in using accelerometers instead. Accelerometers are not affected by steady loads, they can be made comparatively free from interaction effects, and each is a self-contained unit which can be adjusted once and for all before assembly on the model. It was found that there is plenty of flexibility on the model-support system to give a measurable amount of response to applied forces, even in the case of roll, where the design was made as stiff as possible.

There are three accelerometers, two angular and one linear, and the principles of operation are shown in Fig. 4. In each case a moving block is mounted on steel-wire supports to give the required freedom of movement and spring stiffness, and the displacement is measured by means of a variable-gap capacity pick-up. Standard frequency-modulation units convert the capacity variations to voltage signals.

The three accelerometers are designed to have about the same natural frequency (80 to 90 c/s) so that any frequency corrections will be the same for each. The damping is small, so that phase errors at working frequencies do not exceed about 0·2°: these too are nearly equal for the three accelerometers.

The position of the reference axis, at which the vertical acceleration is measured, is chosen so that it is never far from the axis about which the model is oscillating in the pitching (or yawing) mode; this makes the pitching oscillations more nearly equivalent to motion with one degree of freedom. It is not usually possible to place the linear accelerometer at this position, and a potentiometer circuit is therefore provided, as in Fig. 3, which adds a certain proportion of the signal from the angular accelerometer to the signal from the linear accelerometer. This gives a new effective position for the linear accelerometer, which can be made to coincide with the required reference-axis position by suitable adjustment of the potentiometer.

The three accelerometer voltage signals, together with the exciter current signal, are compared in pairs by means of a phasemeter, which measures differences of level and phase angle. This instrument, which is described in Appendix I, has special arrangements for measuring small phase angles, and a tunable filter which largely eliminates the effects of harmonics or distortion in the signals.

Typical numerical examples of complete sets of measurements are given in Tables 4 and 5, together with the results derived from these by the method described in Section 4.2.2 below.

(i) *Static measurements.*—Steady forces and moments (with the model stationary) are measured by means of conventional wire resistance strain gauges mounted on the longitudinal members (for pitching or yawing moment) and on the flat strip (for normal or side force). The construction of the spring unit is such that the force and moment can conveniently be separated in this way; calibrations confirm that interactions, at least under symmetrical loading, are small. The strain gauges are connected to the standard 8 ft tunnel data-recording system.

No measurements of static rolling moment are made since this can be done more conveniently on the spring unit designed for rolling oscillations (Section 7.1).

4.2. *Analysis of Results.*

4.2.1. *One degree of freedom.*—The method of obtaining the required derivatives from the measurements can best be illustrated by considering first the simple case with one degree of freedom. For a pure yawing oscillation, for instance, the equation of motion is

$$(\omega^2 I_{zz} + j\omega N_{\dot{\psi}} + N_{\psi})\psi + N_e = 0 \tag{1}$$

where I_{zz} is the model moment of inertia about the yaw axis, ψ the angular displacement in yaw, ω the frequency in radians per second, N_e the excitation yawing moment, and $N_{\dot{\psi}}$ and N_{ψ} are the damping and stiffness required. These derivatives include both mechanical (structural) and aerodynamic components. If measurements are made with wind on and wind off, the differences $\Delta N_{\dot{\psi}}$ and ΔN_{ψ} are assumed to represent the aerodynamic derivatives required. (*See* below, Sections 5.1 and 5.5.1.)

The only measurements needed in this case are the frequency ω and the ratio of excitation couple to angular acceleration, measured as a vector

$$(N_e/\ddot{\psi}) = (N_e/\ddot{\psi})_{\mathrm{r}} + j(N_e/\ddot{\psi})_{\mathrm{i}} \tag{2}$$

where suffixes r and i represent the real (in-phase) and imaginary (quadrature) components of the vector.

The inertia I_{zz} can be obtained from a previous calibration (*see* below Section 4.3.1), and separating the real and imaginary parts of equations (1) and (2) gives the following equations for the derivatives:

$$N_{\psi} = \omega^2(N_e/\ddot{\psi})_{\mathrm{r}} - \omega^2 I_{zz} \tag{3}$$

$$N_{\dot{\psi}} = \omega(N_e/\ddot{\psi})_{\mathrm{i}} \tag{4}$$

since $\ddot{\psi} = -\omega^2\psi$.

4.2.2. *Two degrees of freedom.*—With two degrees of freedom, there are two equations of motion, each associated with a particular force or moment. As a specific instance, we shall take yawing and sideslip motion, with separate equations for yawing moment and side force.

(i) *Yawing moment.*—The equation of motion, neglecting second-order terms, is

$$(\omega^2 I_{zz} + j\omega N_{\dot{\psi}} + N_{\psi})\psi + (\omega^2 W\bar{x} + j\omega N_{\dot{y}} + N_y)y + N_e = 0 \tag{5}$$

where $W\bar{x}$ is the mass moment of the model, y the sideways displacement, and $N_{\dot{y}}$ and N_y are (total) cross derivatives.

In this case measurements of frequency and amplitude ratio are made in each of the two natural modes, (*a*) (yawing) and (*b*) (predominantly sideslipping), making six measurements in all:

$$\omega_{\mathrm{a}} \quad \omega_{\mathrm{b}} \quad (N_e/\psi)_{\mathrm{a}} \quad (N_e/y)_{\mathrm{b}} \quad (y/\psi)_{\mathrm{a}} \quad (\psi/y)_{\mathrm{b}}$$

where suffixes a and b denote measurements in the corresponding modes, and the quantities in brackets ( ) are all measured as vectors. If these values, together with the inertias I_{zz} and $W\bar{x}$, are substituted in equation (5), then separating real and imaginary parts gives four simultaneous equations for determining the four derivatives N_{ψ}, $N_{\dot{\psi}}$, N_y and $N_{\dot{y}}$ (*see* Appendix II).

The aerodynamic component of N_y must be zero, and any apparent change in N_y between wind-on and wind-off conditions must be attributed to an aerodynamic $N_{\dot{y}}$ (virtual inertia),

producing the same effect as a change in $W\bar{x}$. The value of this $N_{\dot{y}}$ could be obtained by treating N_y as known and $W\bar{x}$ as unknown in the wind-on case, but it is simpler to obtain ΔN_y in the ordinary way, and then write

$$\Delta N_y = \omega_b{}^2 \Delta W\bar{x} = -\omega_b{}^2 \Delta N_{\dot{y}} \tag{6}$$

which in practice gives exactly the same result.

(ii) *Side force.*—The corresponding side-force equation is

$$(\omega^2 W\bar{x} + j\omega Y_{\dot{\psi}} + Y_{\psi})\psi + (\omega^2 W + j\omega Y_{\dot{y}} + Y_y)y + Y_e = 0 \tag{7}$$

where W is the mass of the model and Y_e the side-force excitation. The four derivatives Y_y, $Y_{\dot{y}}$, Y_{ψ}, $Y_{\dot{\psi}}$ can be obtained from the same measurements as before, by using different constants in the equations (Appendix II). (The excitation terms N_e and Y_e are obtained from the same readings of the exciter current, but with different calibration factors.)

The remarks on N_y above apply equally to Y_y.

(iii) *Rolling moment.*—The rolling-moment equations could be set out in a similar way, using L_e to represent a roll balance reaction instead of an excitation rolling moment. Since, however, a correction would then have to be applied to allow for the small rolling motion, it is simpler to start from the complete equation for three degrees of freedom and then introduce simplifications. This complete rolling-moment equation is

$$(-\omega^2 I_{zx} + j\omega L_{\dot{\psi}} + L_{\psi})\psi + (-\omega^2 W\bar{z} + j\omega L_{\dot{y}} + L_y)y + (\omega^2 I_{xx} + j\omega L_{\dot{\phi}} + L_{\phi})\phi = 0 \tag{8}$$

in which ϕ is the angle of roll displacement, and I_{zx}, $W\bar{z}$ and I_{xx} are the product of inertia, mass moment, and moment of inertia of the model, respectively. The four derivatives to be measured are $L_{\dot{\psi}}$, L_{ψ}, L_y, $L_{\dot{y}}$.

In the third expression in equation (8) the roll angle ϕ is small (*see* example in Table 5, and the mechanical roll stiffness L_{ϕ} is so large that the aerodynamic component can be neglected and the damping term $L_{\dot{\phi}}$ can be omitted altogether. If then the natural rolling frequency is designated ω_3, where $\omega_3{}^2 I_{xx} + L_{\phi} = 0$, we may replace the third expression in equation (8) by an effective excitation term

$$L_e = \{1 - (\omega/\omega_3)^2\} L_{\phi}\phi . \tag{9}$$

The term in brackets { } may be treated as a correction factor to a stiffness L_{ϕ} obtained from a calibration test. For any one mode the variations in ω are small, and this factor may be assumed constant, although its value is different for different modes.

Equation (8) now becomes

$$(-\omega^2 I_{zx} + j\omega L_{\dot{\psi}} + L_{\psi})\psi + (-\omega^2 W\bar{z} + j\omega L_{\dot{y}} + L_y)y + L_e = 0 \tag{10}$$

which is of the same form as (5) or (7), and the derivatives L_{ψ}, $L_{\dot{\psi}}$, L_y, $L_{\dot{y}}$ can be obtained from four simultaneous equations as before. L_e is now measured as a roll displacement (or acceleration/ω^2) instead of an exciter current.

4.3. *Calibrations.*

Before the values of the measurements can be used in the equations given above, calibration tests must be made to determine

(i) the various inertias, I_{yy}, $W\bar{x}$ etc.

(ii) the factors to convert transducer voltages to forces or accelerations.

The determination of these constants is one of the most important parts of the experiment, and the technique which has been developed is worth describing in some detail. The main principle is that the calibrations are made dynamically in conditions approximating as closely as possible to those in the actual tests, with the same measuring instruments, the same excitation, and the same amplitudes of vibration.

4.3.1. *One degree of freedom.*—As before, a system with one degree of freedom illustrates the method in its simplest form. The relevant equations are (3) and (4) above. To obtain the inertia I_{zz}, we add weights to the model to give known increments ΔI_{zz} in I_{zz} and in each case measure the resonant frequency ω defined by $(N_e/\ddot{\psi})_r = 0$. Equation (3) then becomes

$$I_{zz} + \Delta I_{zz} + N_\psi/\omega^2 = 0 \tag{11}$$

and a plot of $1/\omega^2$ against ΔI_{zz} will give a straight line from which I_{zz} can immediately be found, and also the mechanical stiffness N_ψ.

It is difficult to make accurate changes in ΔI_{zz} on a typical model, and for these tests the model is replaced by a calibrating frame with facilities for adding known weights in known positions. The above procedure will then give the value of N_ψ (mechanical stiffness) of the system, and a further measurement with the model on will then give the model I_{zz} in terms of the known N_ψ.

To obtain the excitation yawing moment from the current in the vibration generator, we require the factor k to convert a measured voltage ratio v to the ratio $(N_e/\ddot{\psi})$. Then if we write $v = v_r + jv_i$, and assume for the moment that k is a scalar factor, equation (3) becomes

$$I_{zz} + N_\psi/\omega^2 = kv_r \tag{12}$$

so that if we measure v_r for a range of values of ω on either side of resonance, a plot of v_r against $1/\omega^2$ gives a straight line. From the slope of this line k can be determined when N_ψ is known. It is important to maintain a constant amplitude for these tests, to ensure that N_ψ remains constant.

From equation (4),

$$N_{\dot{\psi}} = k\omega v_i \tag{13}$$

which shows that ωv_i should be constant in these tests. If this is not the case, k is not a scalar factor, but a transfer function with a phase angle given by the slope of the line v_i plotted against v_r.

In practice there usually is a phase angle between the exciter current and the exciter force, arising from the flexibility of the driving rod in conjunction with the internal damping of the vibration generator. (*See* Appendix I, Section 2.) This phase error is proportional to frequency, and is corrected by the circuit shown in Fig. 3, which is adjusted until ωv_i is independent of ω.

This excitation calibration, for which no added weights are required, is more conveniently done on the model than on the calibration frame.

4.3.2. *Two degrees of freedom.*—For a system with two degrees of freedom, the same methods are used. Measurements of natural frequencies of the calibrating frame, with systematic increments in the various inertias involved, give the values of the corresponding stiffnesses and inertias, and from these the values of the displacement ratios such as ψ/y can be calculated and used to obtain the calibration factors for the accelerometers. Tests on the model then give the required model inertias and (by exciting off resonance) the excitation factors.

The relevant equations are (5) and (7) above, but for most calibrations they can be considerably simplified by omitting damping and excitation terms. Further details are given in Appendix III.

(i) *Position of reference axis.*—It has already been explained (Section 4.1.3 above) how the position of the reference axis may be changed by adjusting the potentiometer shown in Fig. 3. The usual procedure is to oscillate the model in the (a) mode and to adjust the potentiometer to make the 'linear corrected' signal small. This ensures that the reference axis is near the axis of oscillation in this mode.

It is then necessary to measure the physical position of this reference axis. This can be done in the course of the tests with the calibration frame, by comparing the amplitude ratio ψ/y given by the accelerometers with that calculated from the known stiffnesses and inertias of the system. Details are given in Appendix III, Section 3. Alternatively, the amplitude ratio can be measured by visual observation of the calibrating frame to determine the position of the oscillation axis, which is fairly clearly defined in the (a) mode wind-off case (*see* Appendix III, Section 1). A travelling microscope with a 2 inch objective is suitable for this purpose, and a piece of squared paper makes a convenient viewing surface. This optical method provides a useful check on the other calibrations.

(ii) *Roll calibrations.*—The purpose of the roll calibration is to give the factors to convert measured voltage ratios from the transducers for ϕ, ψ and y to the ratios L_e/ψ and L_e/y, where L_e is the equivalent excitation couple defined by equation (9).

The calibrating frame is used for these tests. To obtain the factor for L_e/ψ, two measurements are made in the (a) mode (yawing), with equal and opposite increments in the product of inertia I_{zx}, keeping all other inertias constant. The mechanical coupling derivatives L_ψ, $L_{\dot{\psi}}$, L_y, $L_{\dot{y}}$ are all small, and it is found that most of the terms in equation (10), including ω, remain constant, so that we may write

$$\omega^2 \Delta I_{zx} = \Delta(L_e/\psi)_r \tag{14}$$

from which the required factor can be immediately determined. Similarly the factor for (L_e/y) may be obtained by changing $W\bar{z}$ and measuring in the (b) mode.

To obtain the frequency-correction term $\{1 - (\omega/\omega_3)^2\}$, it is necessary to measure the natural rolling frequency ω_3 for both the calibrating frame and the model, which can be done by exciting roll oscillations by means of an auxiliary vibration generator. The appropriate modifications can then be made to the calibration factors for the frequencies at which the tests are made.

The values of the model inertias I_{zx} and $W\bar{z}$ can be obtained if necessary, but it is usually permissible to assume that both are zero. Any errors introduced by this assumption will have practically the same effect on the wind-off and wind-on values of L_ψ and L_y, and the differences which give the aerodynamic derivatives will not be affected.

5. *Assessment of Method.*

It is not possible at this stage to give a precise figure for the accuracy attainable in these tests, but this section describes in general terms the main features affecting the reliability of the results. Some of these points are illustrated by the numerical examples of test readings given in Tables 4 and 5. Conclusions can also be drawn from the consistency and repeatability of the results, and in some cases from the agreement between static and dynamic values of the derivatives, where the frequencies are low enough to approximate to quasi-static conditions.

5.1. *Direct Stiffness.*

Direct stiffness derivatives are measured as changes in frequency. There is no difficulty in achieving a high precision in these frequency measurements, but it is important that the mechanical stiffness should remain constant.

In pitch or yaw tests the flexibility comes mainly from the spring unit, which is made in one piece, and no significant variations in the mechanical stiffness occur. Further confirmation of the reliability of the results comes from the agreement between static and dynamic values of the derivatives m_θ and n_ψ, which is generally good. In Fig. 19, however, the dynamic values of m_θ at supersonic speeds are consistently lower than the static. It seems unlikely that this is a true aerodynamic effect, since the frequency parameters are low, but the differences are rather too large to be attributed to known experimental errors. No explanation can at present be given, but further tests on different models may provide more information.

For heave or sideslip tests the aerodynamic derivatives are very small. For the conditions of Table 4, if we assume that $z_{\dot{z}}$ is of the same order as $z_{\dot{\theta}}$, i.e. 0·15 (*see* Fig. 21), the corresponding ΔZ_z (wind-on − wind-off) would be about 15 lb/ft, or 0·08% of the mechanical stiffness. The measured change is 115 lb/ft or 0·62%, which can easily be attributed to a change in the mechanical stiffness, probably due to lack of solidity in the various joints in the sting and its support system, some of which are heavily loaded in the wind-on case. It is not possible in this case to obtain reliable measurements of the aerodynamic ΔZ_z.

5.2. *Direct Damping.*

Direct damping is measured in terms of the excitation, and in the angular modes the mechanical damping is small, so that there is no difficulty in getting good accuracy in measurements of the aerodynamic damping.

In the linear modes the mechanical damping, although still usually smaller than the aerodynamic damping, shows some variation, which is attributable to the fixation changes mentioned above. This is responsible for the scatter in $z_{\dot{z}}$, and in the case of $y_{\dot{y}}$ where the aerodynamic damping forces are very small, the results are not worth plotting.

5.3. *Cross Derivatives.*

Cross derivatives are measured as acceleration ratios and phase angles, the in-phase component giving the cross stiffness and the quadrature component the cross damping. These can be considered separately, with rolling-moment derivatives as a special third category.

5.3.1. *Cross stiffness.*—The acceleration ratio giving Z_θ is the distance from the reference axis to the oscillation axis in the pitching (a) mode, and typical values are plotted in Fig. 7. This distance is small in the wind-off case, and the difference between wind-off and wind-on can be measured with good accuracy.

The acceleration ratio giving M_z is measured as the reciprocal of the distance between the reference axis and the oscillation axis in the heaving (b) mode: this value is not small in the wind-off case (because of the comparatively large component of pitching oscillation) and the change with wind-on is difficult to measure accurately (*see* Fig. 7). Arrangements can be made to avoid this source of error (*see* 7.2 below) but other errors in this derivative can be introduced by variations in the mechanical cross stiffness.

Thus, for the example of Table 4, assuming that $m_{\dot{z}}$ is of the same order as $m_{\dot{\theta}}$, the value of ΔM_z (wind-on − wind-off) should be of the order of − 18 lb, instead of 178 lb as measured. This difference cannot be entirely due to inaccuracy in measurement of the acceleration ratio, and must represent changes in the mechanical cross stiffness M_z. It does not seem to be possible to measure the small aerodynamic effects.

It is known that for a conservative mechanical system the two cross stiffnesses Z_θ and M_z must be equal, showing that the change in mechanical M_z must be accompanied by a similar change in Z_θ. This would reduce the measured ΔZ_θ of -2232 by about 8% or 9%, and the application of this correction would change z_θ from $-0{\cdot}86$ to $-0{\cdot}79$, which gives much better agreement with the static value (Fig. 23).

5.3.2. *Cross damping.*—The wind-off values (mechanical cross damping) are generally small, but the aerodynamic changes to be measured are also small, particularly for heaving and sideslip motion. All the results show a considerable scatter. In Figs. 9 and 20 a comparison is made between $m_{\dot{z}}$ and m_θ, which should be the same at low incidences (*see* Notation, Section 2). In the low-speed tests in the 8 ft Tunnel the $m_{\dot{z}}$ values tend to be higher, which may possibly be a frequency effect (*see* Section 5.4.2).

5.3.3. *Rolling-moment cross derivatives.*—The cross derivatives for rolling moment due to yaw and sideslip (L_ψ, $L_{\dot{\psi}}$, L_y, $L_{\dot{y}}$) are a special case. There is very little mechanical coupling between roll and yaw, so that the measurements are simple and straightforward, and good results were obtained in the low-speed tests. At high speeds, however, there was a considerable amount of rolling oscillation of the model at its natural frequency in roll (about 32 c/s). The amplitude of these oscillations varied in an irregular manner, thus producing disturbances considerably larger than the signals to be measured. The filter of the phasemeter reduced these enough for satisfactory readings of L_ψ to be obtained, but the residual irregularities made it impossible to measure the small phase angle needed for $L_{\dot{\psi}}$. Part of the difficulty arises because these rolling oscillations, being of a higher frequency, were considerably exaggerated by the accelerometer, and later tests on a different model have shown that in this case better results can be obtained from a displacement roll pick-up.

5.4. *Amplitude and Frequency Effects.*

5.4.1. *Amplitude.*—It is known that the mechanical characteristics of the system are to some extent dependent on amplitude, and to minimise errors due to such effects, care has been taken in all these tests to maintain the same oscillation amplitude for wind-on and wind-off tests that are to be compared. This should eliminate this source of error in single-degree-of-freedom tests, but not with two degrees of freedom, because no equation for change of axis position is valid unless all the derivatives are independent of amplitude. Errors due to this cause are expected to be small.

5.4.2. *Frequency.*—The values of both mechanical and aerodynamic derivatives may depend on frequency, but the frequency changes between wind-off and wind-on are always quite small, and no errors from this cause are likely to arise in single-degree-of-freedom tests. The frequency in the heaving or sideslip mode is about three times that of the pitching or yawing modes, and any variation in the derivatives would introduce errors in two-degree-of-freedom tests. Here again the effects on pitching and yawing derivatives are expected to be small, since the second-degree-of-freedom results are used only as a correction to these values.

The low-speed measurements of m_θ and $m_{\dot{z}}$, Figs. 8 and 9, cover a wide range of frequency parameter, 0 to $3{\cdot}0$, and in the 8 ft Tunnel results there is an apparent increase in the derivative with frequency. It is considered doubtful whether this effect is genuine, since a lower accuracy is expected at low speeds. Even if present this effect is small, and seems unlikely to be important at realistic values of the frequency parameter.

5.5. *Special Points.*

5.5.1. *Wind-off datum.*—The datum for aerodynamic-derivative tests of this kind should strictly be obtained from measurements in a complete vacuum. This is of course not practicable, and tests in still air have to be used as a datum. There was no measurable difference between results at pressures of one atmosphere and 1/10 atmosphere. The effects of virtual inertia would in any case be small, and the still-air damping, although possibly significant, depends on the viscosity of the air and is independent of pressure within this range.

5.5.2. *Model flexibility.*—No appreciable flexural vibrations in the model could be excited at frequencies up to 100 c/s or more, and it is concluded that at the frequencies of these tests (about 6 and 18 c/s) any model distortion will be the same as in corresponding static tests[3].

6. *Description of Tests on Cambered Ogee Model.*

6.1. *Model.*

The model, shown in Fig. 6, was as far as possible identical with wing No. 17 in a series of shapes tested statically[3] at R.A.E., Bedford. This particular design was among those most closely resembling at that time the geometry of a possible aircraft.

Leading dimensions and details of the model are given in Table 1. In order to provide enough clearance between the sting and the inside of the model, the wing shape was distorted with a conical shroud, four inches diameter at the trailing edge. For the tests on wing 17 in Ref. 3, the corresponding shroud was 2·6 inches diameter, but there are no significant differences in the results of the static longitudinal tests on the two models. It is possible that the larger shroud may have an appreciable effect in the lateral tests, particularly with the fin on, but no comparisons are available for this case.

The model was made of fibreglass, with a steel insert for mounting on the spring unit. The fin was detachable, and some tests were made without the fin, as noted in the figures.

For the main tests, the model and spring unit were mounted on a standard 8 ft Tunnel sting (*see* Fig. 5a), modified in minor details for the attachment of the vibration generator and drive mechanism.

6.2. *Test Conditions.*

Details of the test conditions are given in Table 2. The mechanical system was designed to give a realistic value of the frequency parameter at the highest speeds tested (e.g. $\nu = 0{\cdot}10$ in the pitching tests at $M = 2{\cdot}6$). Since the frequency remained approximately constant throughout, the frequency parameter is considerably larger at lower speeds. In pitch and yaw the amplitude was about $\pm 1°$ (peak) and in heave and sideslip about $\pm 0{\cdot}035$ inches (peak).

Preliminary tests were made in the 13 ft by 9 ft Tunnel (R.A.E., Bedford) at a wind speed of 200 ft/sec, with the model and spring unit fitted to a dummy sting supported on struts (Fig. 5b). The main tests were then made in the 8 ft by 8 ft Tunnel at R.A.E., Bedford, over a range of Mach numbers up to 2·6. Some tests were also made in this tunnel at 200 ft/sec for comparison with the 13 ft by 9 ft Tunnel tests.

No attempt was made to fix transition in any of the tests.

At Mach numbers of 0·8 and above, the incidence was limited to 8° on account of the stresses in the spring unit produced by the steady aerodynamic loads on the model.

For each test condition the static forces and moments were measured for a range of incidence and yaw, and the slopes of the curves so obtained have been compared with the corresponding dynamic derivatives.

6.3. *Presentation of Results.*

The results are presented in Figs. 8 to 29, Table 6 serving as an index. Derivatives which should have approximately equal values (e.g. m_θ and $m_{\dot{z}}$) are grouped together in the table and compared in the appropriate figures. All of the results are given in terms of the reference axis at $0{\cdot}71\ C_0$. The static derivatives were obtained from the slopes of the curves of Figs. 30 to 33; pitching moment and normal force were measured over the same range of incidence as in the dynamic tests but yawing moment and side force were measured only at zero incidence and rolling moment was not measured.

As explained in Section 5, certain derivatives could not be measured satisfactorily; these derivatives are also listed in Table 6, with appropriate comments, but the results are not presented.

6.3.1. *Corrections.*—The values of the geometric incidence (i.e. corrected for spring and sting deflections) for various test conditions are given in Table 3. These corrections have been applied before plotting the results of the static tests (Figs. 30 and 31).

In plotting the results of the dynamic tests, however, nominal (uncorrected) incidence has been used throughout. This avoids difficulties in cross plotting or interpolation when (as is the case in the high-speed tests) results are available at only three values of the incidence.

No corrections for tunnel constraint have been applied; these are small in all the test conditions.

6.4. *Discussion of Results.*

6.4.1. *Low-speed results* ($V = 200\ ft/sec$).

(i) *Longitudinal.*—The stability in pitch is shown in Figs. 8 (m_θ) and 9 ($m_{\dot{z}}$). For the axis used in these tests, at $0{\cdot}71\ C_0$, the model is unstable and the instability increases with increasing incidence. The damping in pitch is shown in Fig. 10. The model is positively damped and the damping increases considerably with incidence. The normal-force slope is given by $-z_\theta$ in Fig. 11, and less accurately by $-z_{\dot{z}}$ in Fig. 12. The value increases with incidence but the measurements are not accurate enough to show the changes occurring near zero lift (about $\alpha = 2°$).

(ii) *Lateral.*—The lateral derivatives show some unusual features at the higher values of the incidence which are probably associated with the development of the flow over this particular wing.

At incidences above about 10° the stability in yaw increases rapidly (Figs. 13 and 14) while the damping in yaw (Fig. 15) falls rapidly, becoming negative at incidences above about 14°. The fin contribution to the stability is roughly constant with incidence, but the contribution to the damping decreases and changes sign at about 18°. Similar characteristics have been observed in independent tests[4] of an uncambered wing of the same planform.

The values of l_ψ (Fig. 17) increase steadily with increasing incidence and there are no serious irregularities within the range tested. The values of $l_{\dot{\psi}}$ (Fig. 18) are small at low values of the incidence and rapidly become increasingly negative at incidences above about 10°. This behaviour is abnormal. The same experimental technique used in other wings has, however, given normal results (i.e. smaller, positive values for $l_{\dot{\psi}}$ which tend to increase with incidence).

6.4.2. *High-speed results.*

(i) *Longitudinal.*—Values of m_θ and $\frac{1}{2}d\,C_m/d\alpha$ are plotted in Fig. 19. A considerable increase in stability occurs between subsonic and supersonic speeds, the rearward movement of the aerodynamic centre (at $\alpha = 0$) between $M = 0{\cdot}2$ and $M = 1{\cdot}4$ being about $0{\cdot}06\ C_0$. At the highest speeds and incidences tested a 'pitch up' occurs. This can be seen most clearly in the results of the static

measurements (Fig. 30). At supersonic speeds the static values of m_θ are about 0·01 more positive than the dynamic values (Fig. 19), corresponding to an apparent difference of about 0·01 C_0 in the position of the aerodynamic centre, but it is doubtful whether this effect is genuine (*see* Section 5.1). The increase in stability between subsonic and supersonic speeds can also be seen in the values of $m_{\dot{z}}$ (Fig. 20) although the results are very scattered.

Values of $m_{\dot{\theta}}$ are plotted in Fig. 22. The damping is positive throughout the range tested and tends to increase in the conditions in which the pitch up occurs.

(ii) *Lateral.*—The incidence was restricted to 8° for the high-speed tests and no serious abnormalities {such as those described in Section 6.4.1 (ii)} were encountered.

The stability in yaw (Fig. 25) increases near $M = 1$ and then falls gradually to zero at $M = 2{\cdot}6$. The damping in yaw is positive throughout the range (Fig. 26).

The values of l_ψ (Fig. 29) increase with incidence over the whole range of Mach number. Maximum values occur around $M = 2$ and at $M = 2{\cdot}6$ the values are falling rapidly with Mach number.

As explained in Section 5.3.3 it was not found possible to obtain measurements of $l_{\dot{\psi}}$. The low-speed results indicate that over the range of incidence covered the values of $l_{\dot{\psi}}$ are probably small, and this may have contributed to the difficulties of measurement.

7. *Further Developments.*

7.1. *Rolling Tests.*

The equipment for measuring oscillations in roll is now ready for commissioning. The spring unit is shown diagrammatically in Fig. 34, and the excitation is provided by twisting the driving rod by means of a suitable linkage from the vibration generator.

The method of test will be similar to that already described in this report, and it should be possible to measure the derivatives n_ϕ, $l_{\dot{\phi}}$, $n_{\dot{\phi}}$, $l_{\dot{\phi}}$ and possibly y_ϕ and $y_{\dot{\phi}}$. The system will have essentially one degree of freedom, and testing and analysis will be simpler, but in the calibrations it will probably be necessary to include three degrees of freedom.

7.2. *Cross Stiffness M_z.*

This derivative is obtained from the change in the position of the oscillation axis in the heaving (b) mode, and it is explained in Section 5.3.1 that it is difficult to determine this accurately when the measurements are made from the usual reference axis, since the changes are comparatively small. If a second linear accelerometer pick-up is provided, giving a signal of opposite sign, this can be used with a suitable potentiometer, also connected as in Fig. 3, to give a subsidiary reference axis near the (b) mode oscillation axis. In this way it is possible to make more accurate measurements of the change in the position of the oscillation axis, thus removing one of the limitations to the accuracy of measuring M_z.

A more important limitation is variation of the support fixation, and an attempt is being made to improve this on the new spring unit described below (Section 7.3), by eliminating the forward sting joint, which is highly stressed. It is probable, however, that nothing short of a redesign of the sting and quadrant system in the tunnel would completely solve the problem.

7.3. *Combined Yaw-Roll Unit.*

One disadvantage of the present method of test is that two completely different units are needed for yaw-sideslip tests and for rolling tests. A new spring unit with freedom in both yaw and roll is

therefore being designed and made. This will give a system with three degrees of freedom (including the flexibility of the sting), and a suitable driving linkage will be provided so that any of the three natural modes may be excited by using the appropriate frequency.

In the light of experience now gained, there would seem to be no great difficulty in dealing with the additional complications, in measurement and analysis, of this more sophisticated system. The saving in tunnel time will be considerable, and there will be certain other advantages, such as the ability to damp out unwanted roll when measuring yawing oscillations (*see* Section 5.3.3 above).

8. *Conclusions.*

The method described in this report has proved suitable for measuring oscillatory derivatives on conventional sting-mounted models at Mach numbers up to 2·6. Satisfactory measurements were made of direct and cross derivatives for motion in pitch and yaw. For linear motions the derivatives measured were unreliable because of small variations in the characteristics of the model-support system.

The cambered ogee wing tested in this way showed unusual lateral characteristics at high incidences, such as a large loss of damping-in-yaw and a large negative $l_{\dot{\psi}}$.

REFERENCES

No.	*Author(s)*	*Title, etc.*
1	J. B. Bratt	Wind-tunnel techniques for the measurement of oscillatory derivatives. A.R.C. R. & M. 3319. August, 1960.
2	B. H. Beam	A wind-tunnel test technique for measuring the dynamic rotary stability derivatives at subsonic and supersonic speeds. N.A.C.A. Report 1258. 1956.
3	C. R. Taylor	Measurements at Mach numbers up to 2·8, of the longitudinal characteristics of one plane and three cambered slender 'ogee' wings. A.R.C. R. & M. 3328. December, 1961.
4	~~R. L. Maltby and~~ A. Spence ..	Some low speed problems of high speed aircraft. *J. R. Ae. Soc.*, Vol. 66, No. 616, pp. 211 to 225. April, 1962.

4 R.L. Maltby & A Spence Paper delivered to Roy Aero Soc Feb. 1962 (not published)
Information for Mr Spence Feb 1965

APPENDIX I

Details of Components

The following components are described in this Appendix:

1. Spring unit
2. Vibration generator
3. Power amplifier
4. Oscillator
5. Feedback amplifier
6. Counter
7. Accelerometers
8. Force and displacement pick-ups
9. Frequency modulation units
10. Phasemeter.

1. *Spring Unit.*

The spring unit illustrated in Fig. 2 consists of a crossed-spring centre with unequal arms. There are two longitudinal spring strips 9·5 inches long by 0·6 inches deep by 0·4 inches wide, and one vertical strip 1·6 inches long by 0·05 inches thick by 1·2 inches wide. This provides a stiffness of about 65 lb ft per degree, and the springs are designed for a maximum deflection of ±2 degrees. The complete unit is machined out of one piece of high-tensile steel (S.97) to avoid uncertainties in mechanical stiffness or damping due to clamping effects.

2. *Vibration Generator.*

The exciter is a Goodman moving-coil permanent-magnet vibration generator, type 790, with a static force factor of about 10 lb/amp and a nominal maximum thrust of ±35 lb. For the tests described in this report the maximum thrust used was about ±10 lb (peak), giving a force of ± 65 lb in the driving rod. No special cooling was necessary.

The force F produced by the vibration generator may be assumed to be directly proportional to the current in its moving coil, but the driving system, including the vibration generator, driving rod, and linkage, has a certain amount of inertia, damping, and flexibility which constitute an additional degree of freedom. This means that the displacement at the vibration generator differs from that at the model. Since the natural frequency is very high, there is no significant difference in the amplitude of these displacements, but the combination of damping and flexibility gives a phase change, which is treated as a phase difference between the exciting current (or F) and the effective exciting force F'. If λ is the stiffness and K the damping of the excitation system, the phase angle ϵ between F and F' is given by

$$\tan \epsilon = \omega K/\lambda \qquad \text{(AI.1)}$$

which has to be allowed for by the method described in Section 4.3.1.

3. *Power Amplifier.*

A Bryan Savage amplifier model KLF is used, with a nominal output of 1000 watts. This is much more than is needed for the present tests, but the amplifier fulfils the requirement of giving a good output at frequencies down to 3 c/s or even lower.

4. *Oscillator.*

The oscillator is a standard Muirhead model 880A low-frequency decade oscillator, giving a continuously variable frequency from 0·1 to 10,000 c/s, with an output that can be varied from 10 volts downwards by means of a calibrated attenuator. The frequency control is fine enough for the phase angle between displacement and excitation to be adjusted to within $\frac{1}{2}°$ of quadrature even with the comparatively low damping of the unit in the wind-off case.

5. *Feedback Amplifier.*

The circuit of the feedback amplifier is shown in Fig. 35. The phase-shifter consists of a resistance-capacity bridge, adjusted by means of ganged variable resistors and by switching in different condensers. The potentiometer inputs to the output stage give an adjustable gain for either positive or negative damping (the latter was never used in these tests). The output is fed to the power-amplifier input in series with the output from the variable-frequency oscillator. A tripping relay closes the contact S1, thus shorting the oscillator output, and at the same time opens S2, thus putting on maximum positive damping, irrespective of the potentiometer setting.

6. *Counter.*

The electronic timer used for these tests is an 'Advance' transistorised counter type T.C.1, which measures the time in microseconds for one (or alternatively ten) cycles of the input signal. For accurate results it is important for the signal to have a good (or at any rate a constant) wave form, and this is obtained from an auxiliary output from the oscillator, giving a constant level of 10 volts.

7. *Accelerometers.*

7.1. *Design.*

The linear accelerometer in Fig. 4a consists of a cylindrical block 1 inch diameter by 1 inch long, mounted on four steel wires (0·036 inches diameter and 0·875 inches long) perpendicular to its axis. The block is thus constrained to move in the direction of its axis under a spring restoring force. The pick-up consists of the variable-gap condenser formed by an insulated plate and one end of the block. The gap is about 0·010 inches, and the natural frequency of the block on its wires is 85 c/s. To minimise temperature effects, all the metal parts of the accelerometer are steel.

In the angular accelerometer for pitch or yaw shown in Fig. 4b, four wires are arranged to form a pair of spring centres, defining an axis of rotation and providing a spring control. In this case the condenser gap is about 0·007 inches, and the natural frequency is also 85 c/s.

The angular accelerometer for roll is generally similar to that for pitch or yaw, but about half the size and shaped to fit the space available. On this accelerometer the gap had to be reduced to about 0·002 inches to obtain the required sensitivity. This caused trouble because of excessive viscous air damping, which was cured by cutting grooves in the surface of the fixed condenser plate to allow the air to flow in and out more freely. The natural frequency of this accelerometer is about 80 c/s.

7.2. *Adjustments.*

It is important that the c.g. of the moving block in an angular accelerometer coincides exactly with the axis defined by the spring centres, so that the instrument will not respond to linear accelerations. Adjustable balancing screws are therefore provided on the block, and tests are made by mounting the accelerometer on a suitable vibrating platform, and comparing readings obtained with different orientations.

Similar methods are used to determine the direction of the effective axis of the accelerometer relative to the base by which it is mounted (this applies also to the linear accelerometer) and to verify that the axis coincides with a principal axis of inertia of the block.

7.3. *Phase Angle and Sensitivity.*

When an accelerometer of this kind is used for measurements at a frequency ω well below its natural frequency ω_0, the phase lag ϵ in the instrument depends on its damping, and is given approximately by the equation {identical with (AI.1) above}

$$\tan \epsilon = \omega K/\lambda \tag{AI.2}$$

where K is the damping and λ the stiffness of the moving part of the accelerometer. The value of K/λ can be obtained by measurements of the response of the accelerometer near its natural frequency, a test that can conveniently be made with the accelerometer mounted on the model and with the normal model-excitation system, as follows.

If the frequency ω_0 for maximum response is measured, and also the frequencies ω_1 and ω_2 (above and below resonance respectively) at which the response is $1/\sqrt{2}$ of this maximum value, the damping is given by

$$K/\lambda = (\omega_1 - \omega_2)/{\omega_0}^2. \tag{AI.3}$$

For each of the accelerometers described, the value of the time constant K/λ is between 50 and 60 microseconds, giving phase errors of just over $0{\cdot}1°$ at 6 c/s and $0{\cdot}3°$ at 18 c/s. No corrections are required for these, because they are the same for each instrument, and the excitation phase angle is already taken care of in the calibration described in Section 4.3.1.

The sensitivity, expressed in signal strength per unit acceleration, also depends on the test frequency, being proportional to $1/({\omega_0}^2 - \omega^2)$. It thus changes by about 5% between 6 and 18 c/s but this too is allowed for by the method of calibration.

7.4. *Linearity of Response.*

The sensitivity of a variable-gap pick-up varies inversely as the square of the mean gap; its response is therefore non-linear. It is important, therefore, that the peak amplitude is not too large in relation to the gap, and a ratio of 10% has been taken as the maximum acceptable value. (For most measurements, the ratio has been considerably less.) For this maximum value, the 2nd harmonic content of the signal is about 5%, and the sensitivity is less than 1% greater than for small amplitudes.

8. *Force and Displacement Pick-Ups.*

The original design of the spring unit included pick-ups for measuring forces or displacements, and although these were later superseded for most purposes by accelerometers a brief description may be of interest.

The arrangement is sketched in Fig. 36. The pitch or yaw capacity pick-up is of the variable-area type, to ensure linear response for large movements, and measures the angular deflection of the spring unit. This was satisfactory for the symmetrical loading encountered in pitching tests, but in yawing tests the steady aerodynamic loads made the gaps unequal and thus produced roll-yaw interaction on the pick-up.

The four parallel springs, in conjunction with a variable-gap capacity pick-up, provided a normal or side-force balance. This was unsatisfactory in pitch-heave tests, because steady aerodynamic loads changed the gap and therefore the sensitivity of the balance, involving troublesome corrections.

The roll balance, with two variable-gap pick-ups, made use of the small amount of roll flexibility in the springs forming the lift balance. Some of the earlier results recorded in this report were measured with this balance, and it has also been used in subsequent tests to avoid the difficulties mentioned in Section 5.3.3.

9. *Frequency-Modulation Units.*

Standard Southern Instruments equipment (MR220F and M700L) is used to convert the capacity changes in the pick-ups to voltages. Each pick-up has a separate oscillator, with a frequency of about 2 Mc. These oscillators are mounted at the back of the moving incidence quadrant at the extreme rear end of the sting, and are connected to the pick-ups with miniature coaxial cable about 0·08 inches overall diameter. The cables had to be between 22 ft and 25 ft long, which is just within the maximum length with which the frequency modulation equipment would work satisfactorily.

The changes in oscillator frequency produced by the pick-up are converted to voltages by discriminator-amplifiers, one for each pick-up, the sensitivity being about 0·5 volts per pF.

10. *Phasemeter.*

Voltage ratios and phase differences are measured with a Muirhead Phasemeter, which has a frequency range down to 0·25 c/s. In this instrument the two signals to be compared are passed through two calibrated attenuators and reduced to a standard voltage level by manual adjustment. These two standardised voltages are then added or subtracted to give a direct reading of phase angle on a suitably graduated voltmeter, while the difference in level is obtained from the attenuator readings. For measuring small phase angles, the sensitivity can be increased by stepping up both attenuator outputs equally (when the input signals are strong enough). The effects of harmonics or distortion in the signals are practically eliminated by a tunable filter, which cuts out unwanted frequencies before they reach the voltmeter.

When a phase angle of exactly 90° is required, as, for instance, when adjusting the excitation frequency to give phase resonance, the phasemeter can be used as a null instrument, by comparing the vector sum and difference of the two signals, which are equal when the phase angle is 90°. This is true even if the voltages have not been exactly standardised by setting the attenuators.

APPENDIX II

Equations for Reduction of Results

Equations (5) or (7) can be written more generally as

$$(\omega^2 I_1 + j\omega K_1 + \lambda_1)\xi + (\omega^2 I_2 + j\omega K_2 + \lambda_2)\eta + Q = 0 \qquad \text{(AII.1)}$$

where I, K, λ represent inertia, damping, and stiffness respectively, ξ and η are displacements in the two degrees of freedom, and Q is the excitation force or couple. The significance of these symbols in particular cases is defined in the table at the end of this Appendix. Then from measurements in the two modes (a) and (b) (with predominantly ξ and η displacements respectively), the unknown derivatives K and λ are obtainable from the following simultaneous equations:

$$\lambda_1 = -\omega_a{}^2\{I_1 + I_2(\eta/\xi)_{ar} - (Q/\ddot{\xi})_{ar}\} - (\eta/\xi)_{ar}\lambda_2 + \omega_a(\eta/\xi)_{ai}K_2 \qquad \text{(AII.2)}$$

$$\lambda_2 = -\omega_b{}^2\{I_2 + I_1(\xi/\eta)_{br} - (Q/\ddot{\eta})_{br}\} - (\xi/\eta)_{br}\lambda_1 + \omega_b(\xi/\eta)_{bi}K_1 \qquad \text{(AII.3)}$$

$$K_1 = -\omega_a\{I_2(\eta/\xi)_{ai} - (Q/\ddot{\xi})_{ai}\} - (\eta/\xi)_{ar}K_2 - (1/\omega_a)(\eta/\xi)_{ai}\lambda_2 \qquad \text{(AII.4)}$$

$$K_2 = -\omega_b\{I_1(\xi/\eta)_{bi} - (Q/\ddot{\eta})_{bi}\} - (\xi/\eta)_{br}K_1 - (1/\omega_b)(\xi/\eta)_{bi}\lambda_1 \qquad \text{(AII.5)}$$

in which symbols in plain brackets ( ) represent quantities measured as transducer voltage ratios, with suffixes r, i, a, b, to denote real and imaginary components in the (a) and (b) modes.

These equations are well conditioned, and, expressed in the above form, can be solved by a simple iteration method in two or three stages. These computations are done by DEUCE. The numerical values given in Tables 4 and 5 show the orders of magnitude of the quantities involved.

The following table shows the inertias, displacements, and excitation to be used in the five sets of equations obtainable from the Pitch-Heave and Yaw-Sideslip tests, and also the aerodynamic components of the four derivatives given by each set. In the rolling-moment equations Q is not strictly an excitation but is measured in terms of ϕ or $\ddot{\phi}$ as L_e in equations (9) and (10) {Section 4.2.2 (iii)}.

Motions	Pitch Heave		Yaw Sideslip		
Displacements ξ	θ		ψ		
η	z		y		
Force or moment	Pitching Moment	Normal Force	Yawing Moment	Side Force	Rolling Moment
Excitation Q	M_e	Z_e	N_e	Y_e	L_e
Inertias					
I_1	I_{yy}	$-W\bar{x}$	I_{zz}	$W\bar{x}$	$-I_{zx}$
I_2	$-W\bar{x}$	W	$W\bar{x}$	W	$-W\bar{z}$
Derivatives					
Stiffness λ_1	M_θ	Z_θ	N_ψ	Y_ψ	L_ψ
Stiffness *λ_2	M_z	Z_z	N_y	Y_y	L_y
Damping K_1	$M_{\dot{\theta}}$	$Z_{\dot{\theta}}$	$N_{\dot{\psi}}$	$Y_{\dot{\psi}}$	$L_{\dot{\psi}}$
Damping K_2	$M_{\dot{z}}$	$Z_{\dot{z}}$	$N_{\dot{y}}$	$Y_{\dot{y}}$	$L_{\dot{y}}$

* This is usually treated as an acceleration derivative or virtual inertia (*see* Section 4.2.2.i).

APPENDIX III

Calibrations with Two Degrees of Freedom

1. *Axes.*

In the calibration and reduction of the results, various axes in different fore-and-aft positions are involved, and these are defined as follows.

The *reference axis*, which is the datum for all results, is the effective position of the linear accelerometer, as modified by the potentiometer circuit of Fig. 3 (*see* Section 4.1.3). Angular acceleration about this axis produces no output signal at the terminals marked 'linear (corrected)'.

The *calibrating-frame axis* is used as the datum for inertia changes in tests with added weights, and hence for all stiffnesses and inertias deduced from such tests.

The positions of the two *oscillation axes* for the (a) and (b) modes are defined as the fore-and-aft positions at which the component of the linear oscillation in phase with the angular oscillation is zero. When the damping is small, these are practically the centres of rotation in the two modes. The oscillation axes are not fixed (*see* Fig. 7) and have no significance in the reduction of the results.

The position of the *spring centre* axis is a constructional detail which has no significance in the analysis.

These axes are, in principle, all quite independent, but the reference axis is placed near the oscillation axis in the (a) mode (wind-off), and the axis of the calibrating frame is located at the spring centre.

2. *Stiffnesses.*

From measurements with added weights on the calibration frame it is possible to obtain the stiffnesses of the system and the accelerometer calibrations. For this purpose the equations in Appendix II can be considerably simplified by omitting damping and excitation terms.

For convenience we may write $u = 1/\omega^2$, and the equations for pitch-heave motion then become

$$I_{yy} + uM_\theta = (z/\theta)_r(W\bar{x} - uM_z) \tag{AIII.1}$$

$$W\bar{x} - uZ_\theta = (z/\theta)_r(W + uZ_z) \tag{AIII.2}$$

and elimination of (z/θ) gives the frequency equation

$$(M_\theta Z_z - M_z Z_\theta)u^2 + \{I_{yy}Z_z + WM_\theta + W\bar{x}(M_z + Z_\theta)\}u + I_{yy}W - (W\bar{x})^2 = 0. \tag{AIII.3}$$

The two roots of this equation are the values of $1/\omega^2$ measured as u_a and u_b in the (a) and (b) modes, and we have

$$-(u_a + u_b)(M_\theta Z_z - M_z Z_\theta) = I_{yy}Z_z + WM_\theta + W\bar{x}(M_z + Z_\theta) \tag{AIII.4}$$

$$u_a u_b (M_\theta Z_z - M_z Z_\theta) = I_{yy}W - (W\bar{x})^2. \tag{AIII.5}$$

Since we are dealing with a conservative mechanical system, $M_z = Z_\theta$, and there are thus three unknown stiffnesses M_θ, Z_z, Z_θ which can be obtained by measuring u_a and u_b for a series of known changes in the inertias I_{yy}, W, $W\bar{x}$.

It is convenient to start by changing $W\bar{x}$ in a series of constant increments, keeping I_{yy} and W constant. For the nth increment, $W\bar{x} = (W\bar{x})_0 + n(\Delta W\bar{x})$. A plot of $u_a + u_b$ against n then gives a straight line of slope $-2Z_\theta(\Delta W\bar{x})/(M_\theta Z_z - Z_\theta^2)$, and a plot of first differences $\Delta(u_a u_b)$ against $n + \frac{1}{2}$ gives a straight line of slope $-2(\Delta W\bar{x})/(M_\theta Z_z - Z_\theta^2)$ with a zero value at $n + \frac{1}{2} = -(W\bar{x})_0/(\Delta W\bar{x})$. This gives values of $M_\theta Z_z$, $Z_\theta (= M_z)$, and $(W\bar{x})_0$.

A further series of tests is then made in which I_{yy} and W are altered and $W\bar{x}$ is kept constant. The 'uncoupled frequencies' defined by

$$u_1 = -I_{yy}/M_\theta \tag{AIII.6}$$

$$u_2 = -W/Z_z \tag{AIII.7}$$

are then given in terms of the measured u_a and u_b by the following equations {derived from (AIII.1) and (AIII.2)}

$$u_1 = u_a - (W\bar{x} - u_a Z_\theta)^2/M_\theta Z_z(u_a - u_2) \tag{AIII.8}$$

$$u_2 = u_b - (W\bar{x} - u_b Z_\theta)^2/M_\theta Z_z(u_b - u_1) \tag{AIII.9}$$

in which u_1 and u_2 are the only unknowns. {These equations can be readily solved by iteration, since $(u_1 - u_a)$ and $(u_2 - u_b)$ are both small.} We may now plot u_1 against ΔI_{yy} and u_2 against ΔW to obtain straight lines with slopes $-1/M_\theta$ and $-1/Z_z$ respectively.

The values of the stiffnesses and inertias obtained in this way are all referred to the calibration axis defined above, and require conversion to the reference axis if they are to be used in later analysis (e.g. Section 4 of this Appendix).

3. *Accelerometers.*

The amplitude ratio in the tests described in the preceding section may be calculated from the equations {derived from (AIII.1 and (AIII.2)}

$$(z/\theta)_{ra} = (W\bar{x} - u_a Z_\theta)/Z_z(u_a - u_2) \tag{AIII.10}$$

$$(z/\theta)_{rb} = M_\theta(u_b - u_1)/(W\bar{x} - u_b Z_\theta). \tag{AIII.11}$$

If the values of $(z/\theta)_r$ are plotted against the measured transducer voltage ratio, the points will lie on a straight line with a slope giving the accelerometer calibration factor and an intercept giving the distance h of the reference axis aft of the calibrating-frame axis.

4. *Model Inertias.*

When the calibrating frame is replaced by the model, one set of measurements in the (a) and (b) modes will give the model inertias I_{yy}, W, and $W\bar{x}$. The relevant equations are

$$I_{yy}\left\{1 - \frac{(z/\theta)_a^2}{(z/\theta)_b^2}\right\} = -M_\theta'\left\{u_a - u_b\frac{(z/\theta)_a^2}{(z/\theta)_b^2}\right\} + Z_z(u_a - u_b)\left(\frac{z}{\theta}\right)_a^2 \tag{AIII.12}$$

$$W\left\{1 - \frac{(z/\theta)_a^2}{(z/\theta)_b^2}\right\} = -Z_z\left\{u_b - u_a\frac{(z/\theta)_a^2}{(z/\theta)_b^2}\right\} + M_\theta'(u_b - u_a)\Big/\left(\frac{z}{\theta}\right)_b^2 \tag{AIII.13}$$

$$W\bar{x}\left\{1 + \frac{(z/\theta)_a}{(z/\theta)_b}\right\} = I_{yy}\Big/\left(\frac{z}{\theta}\right)_b + W\left(\frac{z}{\theta}\right)_a. \tag{AIII.14}$$

In these equations (z/θ) denotes $(z/\theta)_r$, the suffix being omitted for clarity. M_θ' is obtained from the stiffness measured in the calibration described above, converted to the reference axis by the relation

$$M_\theta' = M_\theta - 2hZ_\theta + h^2 Z_z. \tag{AIII.15}$$

5. *Excitation.*

The excitation-transducer constant can be obtained by measurements over a small range of frequencies on either side of resonance, as for the single-degree-of-freedom case described in Section 4.3.1, except that instead of equation (12) we use equation (AII.2) re-arranged as follows :

$$kv_r = (Q/\ddot{\xi})_{ar} = [I_1 + (\eta/\xi)_{ar} I_2] + [\lambda_1 + (\eta/\xi)_{ar}\lambda_2]/\omega_a^2 - (\eta/\xi)_{ai} K_2/\omega_a . \qquad \text{(AIII.16)}$$

In this equation I_1 is constant, and the term $(\eta/\xi)_{ai}K_2/\omega_a$ is also practically constant over a small range of ω, so that a plot of

$$\lambda_1/\omega_a^2 + (\eta/\xi)_{ar}[I_2 + \lambda_2/\omega_a^2]$$

against v_r gives a straight line of slope k.

Instead of equation (13) we use a rearrangement of equation (AII.4):

$$kv_i = (Q/\ddot{\xi})_{ai} = [K_1 + (\eta/\xi)_{ar} K_2]/\omega_a + (\eta/\xi)_{ai}[I_2 + \lambda_2/\omega_a^2] \qquad \text{(AIII.17)}$$

and it is found in practice that the right-hand side of this equation is constant for the small range of ω which is used. It follows that v_i should be constant: if this is not the case, a phase correction must be applied by the circuit in Fig. 3. (*See* Appendix I, Section 2.)

Equations (AIII.16) and (AIII.17) apply to measurements in the (a) mode for obtaining excitation calibrations for pitching or yawing moments. For normal or side-force excitation calibrations, measurements are made in the (b) mode, and the appropriate equations may be derived from equations (AII.3) and (AII.5).

APPENDIX IV

Axes Conversion Equations

This appendix gives the equations needed to convert the sting-axes derivatives used in this report to derivatives referred to moving body axes or to vertical-horizontal fixed axes.

1. *Body Axes.*

The following equations may be used to convert sting-axes derivatives to body-axes derivatives. The latter are expressed in the usual form as derivatives with respect to velocity components u, v, w and angular velocity components p, q, r, whose directions are defined by x, y, z axes moving with the model.

Longitudinal

$$
\begin{aligned}
m_u &= m_{\dot{x}} \\
m_w &= m_{\dot{z}} \\
m_{\dot{u}} &= m_{\ddot{x}} \\
m_{\dot{w}} &= m_{\ddot{z}} \\
m_q &= m_{\dot{\theta}} - m_{\ddot{z}} \cos\alpha + m_{\ddot{x}} \sin\alpha
\end{aligned}
$$

and similar equations obtained by replacing m by z or x.

Lateral ($\beta = 0$ only)

$$
\begin{aligned}
n_v &= n_{\dot{y}} \\
n_{\dot{v}} &= n_{\ddot{y}} \\
n_r &= n_{\dot{\psi}} + n_{\ddot{y}} \cos\alpha \\
n_p &= n_{\dot{\phi}} - n_{\ddot{y}} \sin\alpha
\end{aligned}
$$

and similar equations obtained by replacing n by l or y.

2. *Vertical-Horizontal Axes.*

In the following equations, a prime (′) indicates that the forces and displacements are measured relative to a set of fixed axes $x'\,y'\,z'$, the x' and y' axes being horizontal and the z' axis being vertical. The y' axis coincides with the sting y axis, and the x and x' axes differ by the angle of incidence α.

Longitudinal

$$
\begin{aligned}
x'_{x'} &= x_x \cos^2\alpha + (x_z + z_x) \sin\alpha \cos\alpha + z_z \sin^2\alpha \\
x'_{z'} &= x_z \cos^2\alpha + (z_z - x_x) \sin\alpha \cos\alpha - z_x \sin^2\alpha \\
x'_{\theta'} &= x_\theta \cos\alpha + z_\theta \sin\alpha \\
z'_{x'} &= z_x \cos^2\alpha + (z_z - x_x) \sin\alpha \cos\alpha - x_z \sin^2\alpha \\
z'_{z'} &= z_z \cos^2\alpha - (x_z + z_x) \sin\alpha \cos\alpha + x_x \sin^2\alpha \\
z'_{\theta'} &= z_\theta \cos\alpha - x_\theta \sin\alpha \\
m'_{x'} &= m_x \cos\alpha + m_z \sin\alpha \\
m'_{z'} &= m_z \cos\alpha - m_x \sin\alpha \\
m'_{\theta'} &= m_\theta
\end{aligned}
$$

and similar equations obtained by replacing suffixes x, z, θ by $\dot{x}$, $\dot{z}$, $\dot{\theta}$ or $\ddot{x}$, $\ddot{z}$, $\ddot{\theta}$.

Aerodynamic derivatives with respect to x or z are generally zero.

Lateral

$$y'_{y'} = y_y$$

$$y'_{\phi'} = y_\phi \cos\alpha + y_\psi \sin\alpha$$

$$y'_{\psi'} = y_\psi \cos\alpha - y_\phi \sin\alpha$$

$$l'_{y'} = l_y \cos\alpha + n_y \sin\alpha$$

$$l'_{\phi'} = l_\phi \cos^2\alpha + (l_\psi + n_\phi) \sin\alpha \cos\alpha + n_\psi \sin^2\alpha$$

$$l'_{\psi'} = l_\psi \cos^2\alpha - (l_\phi - n_\psi) \sin\alpha \cos\alpha - n_\phi \sin^2\alpha$$

$$n'_{y'} = n_y \cos\alpha - l_y \sin\alpha$$

$$n'_{\phi'} = n_\phi \cos^2\alpha - (l_\phi - n_\psi) \sin\alpha \cos\alpha - l_\psi \sin^2\alpha$$

$$n'_{\psi'} = n_\psi \cos^2\alpha - (l_\psi + n_\phi) \sin\alpha \cos\alpha + l_\phi \sin^2\alpha$$

and similar equations obtained by replacing suffixes y, ϕ, ψ by $\dot{y}$, $\dot{\phi}$, $\dot{\psi}$ or $\ddot{y}$, $\ddot{\phi}$, $\ddot{\psi}$.

Aerodynamic derivatives with respect to y are generally zero and, with vertical-horizontal axes, derivatives with respect to ϕ are also zero. The derivatives with respect to ψ are then given by

$$y'_{\psi'} = y_\psi \cos\alpha$$

$$l'_{\psi'} = l_\psi - n_\phi = l_\psi + n_\psi \tan\alpha$$

$$n'_{\psi'} = n_\psi + l_\phi = n_\psi - l_\psi \tan\alpha$$

These equations do not apply to derivatives with respect to $\dot{\psi}$ or $\dot{\phi}$.

TABLE 1

Model Particulars

Length	(C_0)	5·00 ft
Span	(b)	2·08 ft
Area	(S)	4·68 sq ft
Aerodynamic mean chord	($\bar{c}$)	3·08 ft
Position of reference axis	$0{\cdot}71C_0$	$(= 0{\cdot}53\bar{c})$

TABLE 2

Test Conditions

In the pitching and yawing modes the frequency was approximately 6·5 c/s and the amplitude approximately $\pm 1°$ (peak). In the heaving and sideslipping modes the frequency was approximately 18 c/s and the amplitude approximately $\pm 0{\cdot}035$ in. (peak).

Tunnel	13 ft × 9 ft	8 ft × 8 ft					
Speed (ft/sec) Mach No.	200	200	0·8	1·4	1·8	2·2	2·6
Reynolds No. (Based on C_0)	6×10^6	6×10^6	8×10^6				
$\frac{1}{2}\rho V^2$(lb/sq ft)	47·6	45·9	206	277	280	269	252
Range of incidence	0 to 20°	0 to 20°	0, 4°, 8°				
$\nu = \frac{\omega C_0}{V}$ Pitch	1·0	1·0	0·23	0·14	0·12	0·11	0·10
$\nu = \frac{\omega C_0}{V}$ Heave	3·0	2·7	0·65	0·41	0·34	0·30	0·28
$\nu = \frac{\omega b}{2V}$ Yaw	0·21	0·21	0·049	0·031	0·026	0·023	0·021
$\nu = \frac{\omega b}{2V}$ Sideslip	0·63	0·56	0·13	0·083	0·069	0·062	0·057

TABLE 3

Longitudinal Tests. Values of Geometric Incidence
(i.e. Corrected for Spring and Sting Deflections)

$\alpha_{NOMINAL}$ (degrees)	$V = 200$ ft/sec	M					
		0·8	1·4	1·6	1·8	2·2	2·6
0	0·1	0·5	0·7	0·6	0·5	0·4	0·3
4		4·5	4·3	4·3	4·2	4·1	4·1
5	5·1						
8		8·0	8·0		8·0	8·0	8·0
10	10·2						
15	15·3						
20	20·6						

In the lateral tests at $\alpha_{NOMINAL} = 0$ the corrections to both α and β were negligible.

TABLE 4

Numerical Example: Pitch-Heave Test

	Units	Value	
Constants			
I_{yy}	slugs ft^2	2·15	
$W\bar{x}$	slugs ft	0·89	
W	slugs	1·88	
Measurements		Wind-off	Wind-on
α		0	0
Mach number		0	1·4
V	ft/sec	0	1350
q	lb/ft^2	0	277
Pitching mode			
$\ddot{z}/\ddot{\theta}$	ft	0·0177/π−11°	0·174/π−1·2°
$M_e/\ddot{\theta}$	lb ft sec^2	0·0159/−90°	0·0568/−90°
$Z_e/\ddot{\theta}$	lb sec^2	0·00879/−90°	0·0314/−90°
n	cycles/sec	6·466	6·761
Heaving mode			
$\ddot{\theta}/\ddot{z}$	1/ft	0·422/−0·55°	0·437/−1·4°
$M_e/\ddot{z}$	lb sec^2	0·0156/−90°	0·0376/−90°
$Z_e/\ddot{z}$	lb sec^2/ft	0·00860/−90°	0·0208/−90°
n	cycles/sec	17·388	17·978
Derivatives obtained from above measurements (*see* Appendix II)			
M_θ	lb ft	−3552	−3966
M_z	lb	1290	1112
$M_{\dot{\theta}}$	lb ft sec	−0·64	−2·53
$M_{\dot{z}}$	lb sec	−0·63	−0·92
Z_θ	lb	1202	−1030
Z_z	lb/ft	−18463	−18578
$Z_{\dot{\theta}}$	lb sec	0·89	−0·62
$Z_{\dot{z}}$	lb sec/ft	−1·66	−3·25

TABLE 5

Numerical Example: Yaw-Sideslip Test

	Units	Value	
Constants			
I_{zz}	slugs ft²	2·26	
$W\bar{x}$	slugs ft	0·96	
W	slugs	1·90	
I_{zx}	slugs ft²	0 } *See* Section 4.3.2(ii)	
$W\bar{z}$	slugs ft	0 }	
Measurements		Wind-off	Wind-on
α		0	15°
V	ft/sec	0	200
q	lb/ft²	0	43·2
Yawing mode			
$\ddot{y}/\ddot{\psi}$	ft	$0{\cdot}00706/\pi-28°$	$0{\cdot}00253/\pi+25\frac{1}{2}°$
$N_e/\ddot{\psi}$	lb ft sec²	$0{\cdot}0130/-90°$	$0{\cdot}00951/-90°$
$Y_e/\ddot{\psi}$	lb sec²	$0{\cdot}00690/90°$	$0{\cdot}00506/90°$
$L_e/\ddot{\psi}$	lb ft sec²	$0{\cdot}00355/\pi-26°$	$0{\cdot}0612/-12°$
n	cycles/sec	6·348	6·385
ϕ/ψ		$0{\cdot}0016/\pi-26°$	$0{\cdot}027/-12°$
Sideslipping mode			
$\ddot{\psi}/\ddot{y}$	1/ft	$0{\cdot}415/\pi-0{\cdot}42°$	$0{\cdot}420/\pi-0{\cdot}60°$
$N_e/\ddot{y}$	lb sec²	$0{\cdot}0109/90°$	$0{\cdot}0141/90°$
$Y_e/\ddot{y}$	lb sec²/ft	$0{\cdot}00578/-90°$	$0{\cdot}00750/-90°$
$L_e/\ddot{y}$	lb sec²	$0{\cdot}00152/\pi+6{\cdot}8°$	$0{\cdot}00594/\pi+34°$
n	cycles/sec	17·123	17·117
ϕ/y		$0{\cdot}0068/\pi+6{\cdot}8°$	$0{\cdot}026/\pi+34°$
Derivatives obtained from above measurements (*see* Appendix II)			
N_ψ	lb ft	−3597	−3638
N_y	lb	−1750	−1658
$N_{\dot{\psi}}$	lb ft sec	−0·53	−0·38
$N_{\dot{y}}$	lb sec	0·32	0·44
Y_ψ	lb	−1621	−1579
Y_y	lb/ft	−18055	−17979
$Y_{\dot{\psi}}$	lb sec	−0·98	−0·23
$Y_{\dot{y}}$	lb sec/ft	−1·30	−1·29
L_ψ	lb ft	−5	97
L_y	lb	−20	−17
$L_{\dot{\psi}}$	lb ft sec	0·05	−0·51
$L_{\dot{y}}$	lb sec	0	−0·58

TABLE 6

Summary of Results

Derivative	$V = 200$ ft/sec			$M = 0{\cdot}8$ to $2{\cdot}6$		
	Fig. No.	Remarks		Fig. No.	Remarks	
			Section			*Section*
m_θ	8	Satisfactory	5.1	19	Satisfactory	5.1
$m_{\dot{z}}$	9	Considerable scatter	5.3.2	20	Considerable scatter	5.3.2
$m_{\dot{\theta}}$	10	Satisfactory	5.2	22	Satisfactory	5.2
$m_{\ddot{z}}$	—	Unsatisfactory	5.3.1	—	Unsatisfactory	5.3.1
z_θ	11	Satisfactory	5.3.1	23	Satisfactory	5.3.1
$z_{\dot{z}}$	12	Considerable scatter	5.2	24	Considerable scatter	5.2
$z_{\dot{\theta}}$	11	Considerable scatter	5.3.2	21	Considerable scatter	5.3.2
$z_{\ddot{z}}$	—	Unsatisfactory	5.1	—	Unsatisfactory	5.1
n_ψ	13	Satisfactory	5.1	25	Satisfactory	5.1
$n_{\dot{y}}$	14	Considerable scatter	5.3.2	—	Unsatisfactory	5.3.2
$n_{\dot{\psi}}$	15	Satisfactory	5.2	26	Satisfactory	5.2
$n_{\ddot{y}}$	—	Unsatisfactory	5.3.1	—	Unsatisfactory	5.3.1
y_ψ	—	Unsatisfactory	5.3.1	27	Considerable scatter	5.3.1
$y_{\dot{y}}$	—	Unsatisfactory	5.2	—	Unsatisfactory	5.2
$y_{\dot{\psi}}$	16	Considerable scatter	5.3.2	28	Considerable scatter	5.3.2
$y_{\ddot{y}}$	—	Unsatisfactory	5.1	—	Unsatisfactory	5.1
l_ψ	17	Satisfactory	5.3.3	29	Satisfactory	5.3.3
$l_{\dot{y}}$	17	Satisfactory	5.3.3	—	Unsatisfactory	5.3.3
$l_{\dot{\psi}}$	18	Satisfactory	5.3.3	—	Unsatisfactory	5.3.3
$l_{\ddot{y}}$	—	Unsatisfactory	5.3.3	—	Unsatisfactory	5.3.3

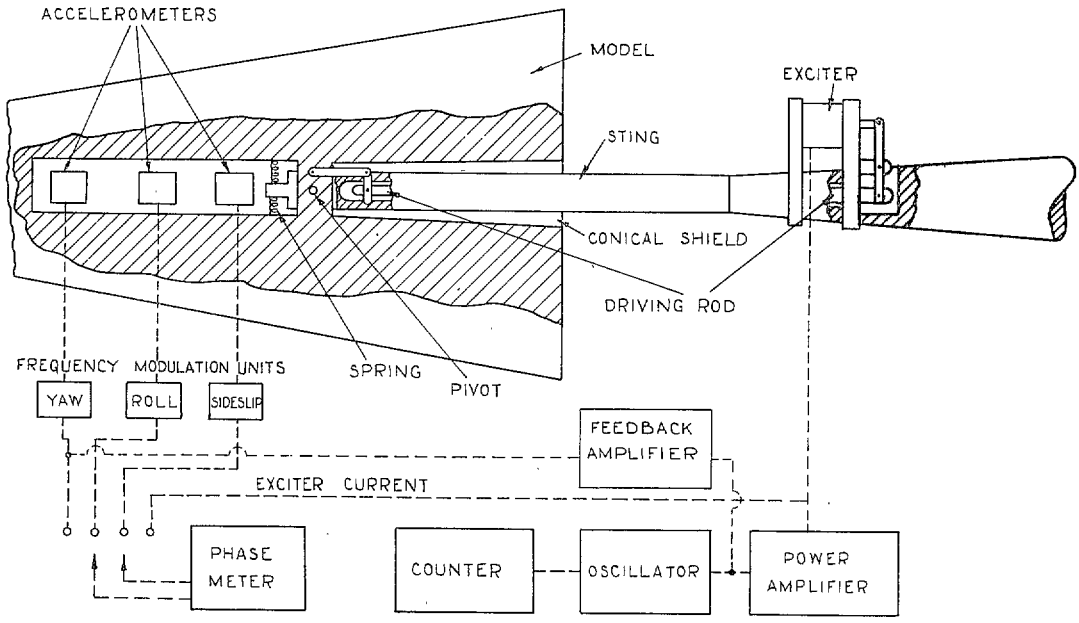

FIG. 1. Schematic arrangement for yaw-sideslip oscillations.

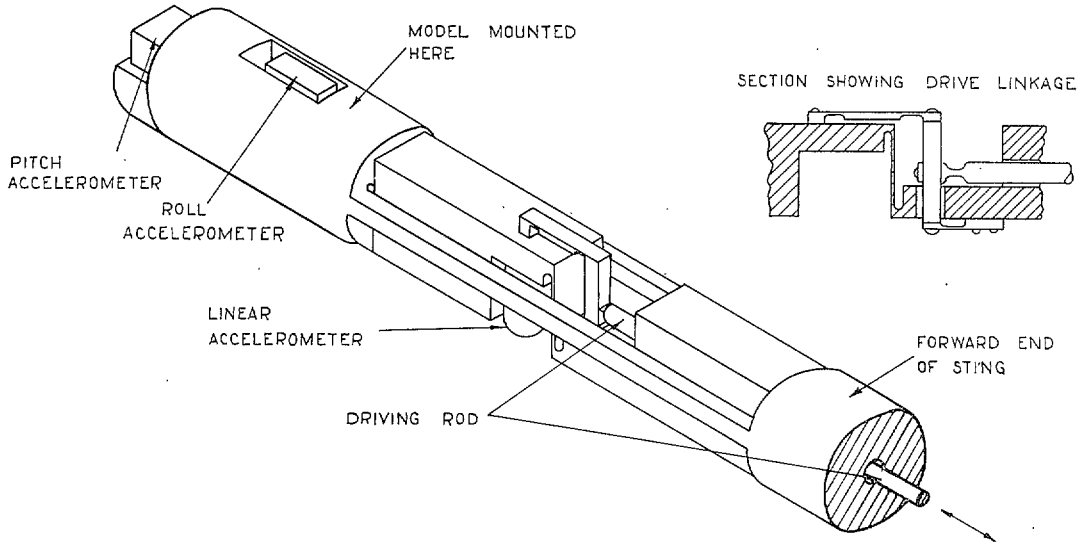

FIG. 2. Pitch or yaw spring unit.

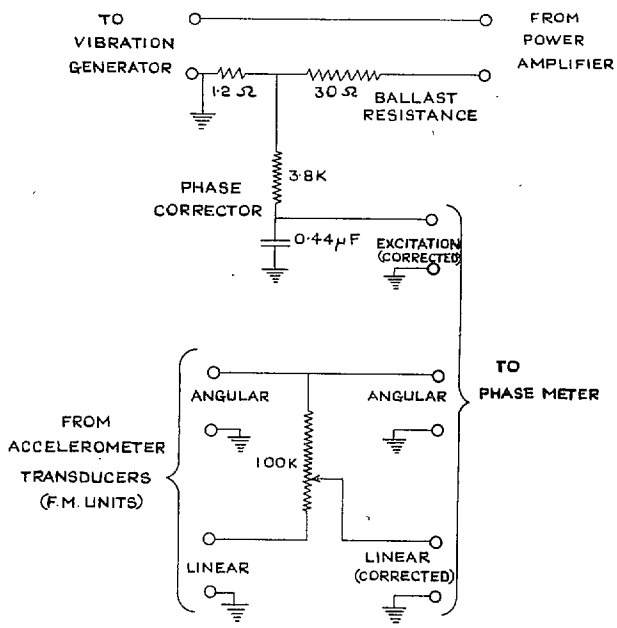

FIG. 3. Circuit details.

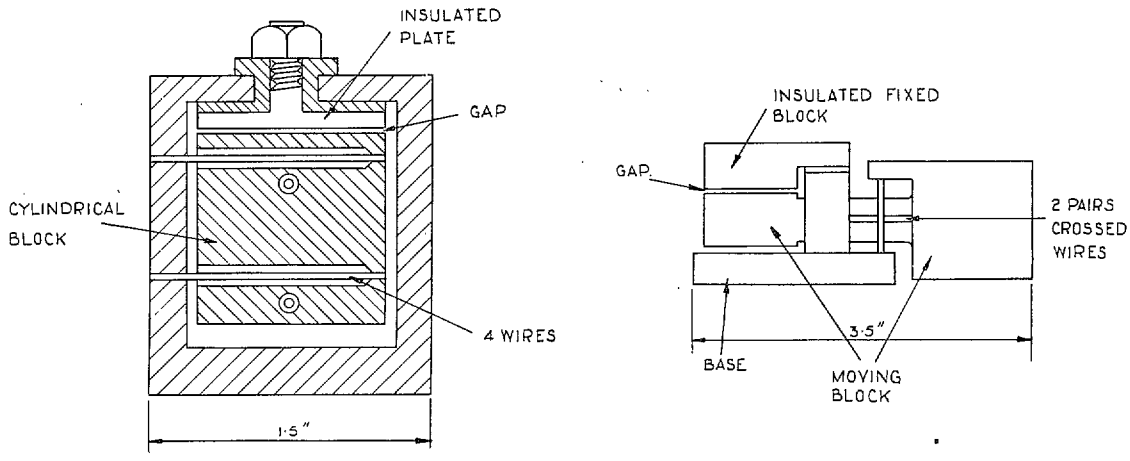

(a) Linear (b) Angular (pitch)

FIG. 4. Accelerometers.

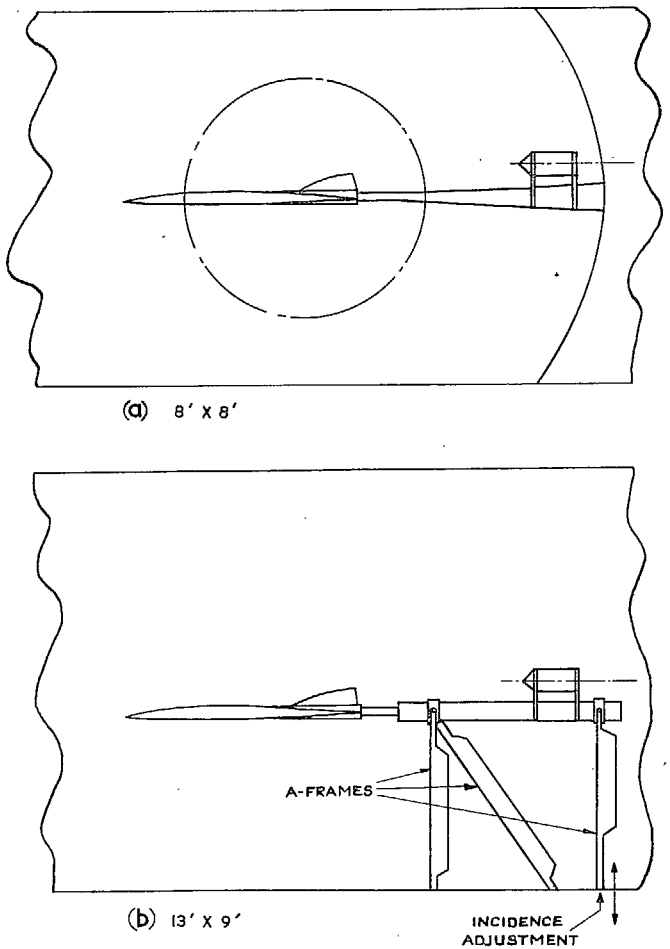

FIG. 5. Tunnel installations.

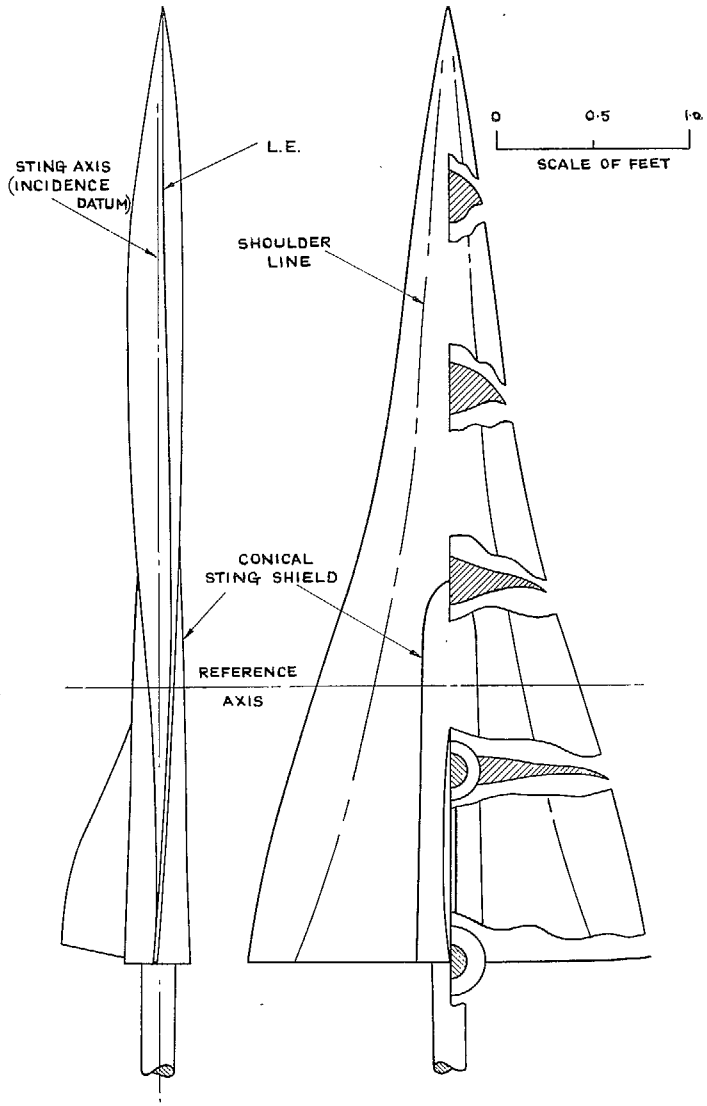

FIG. 6. Cambered ogee model.

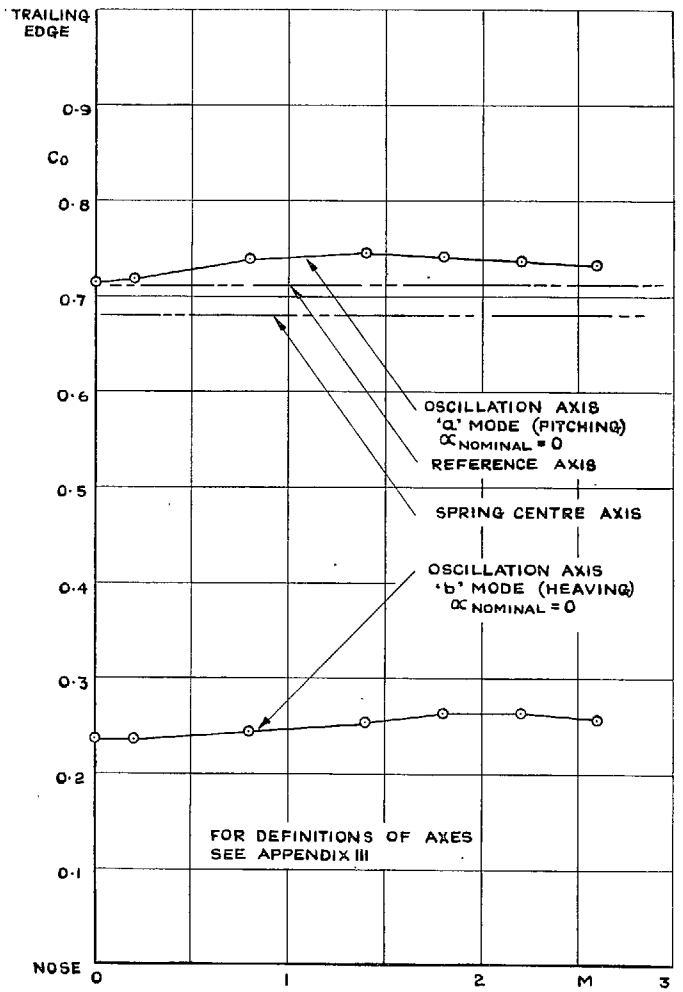

FIG. 7. Positions of axes.

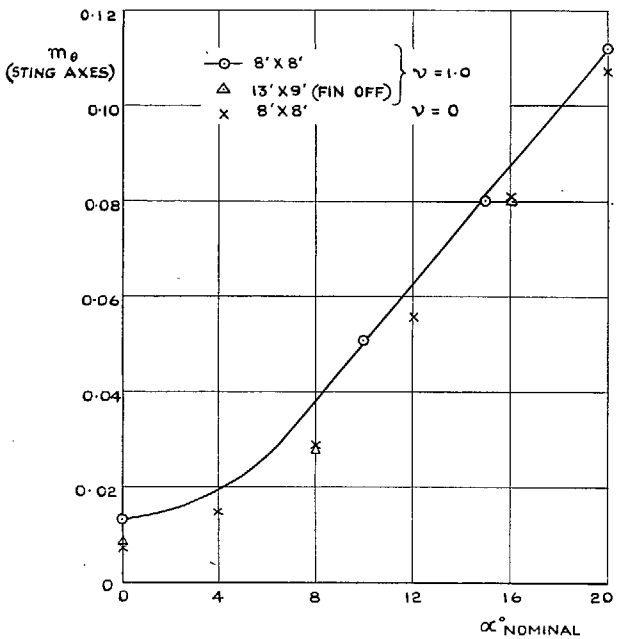

FIG. 8. Stability in pitch, m_θ. Variation with incidence. $V = 200$ ft/sec.

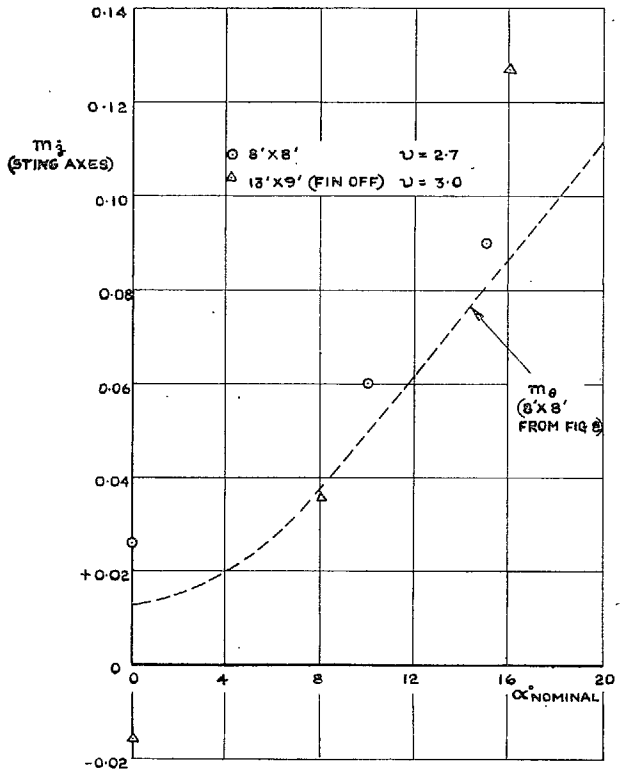

FIG. 9. Stability in pitch, $m_{\dot{\alpha}}$. Variation with incidence. $V = 200$ ft/sec.

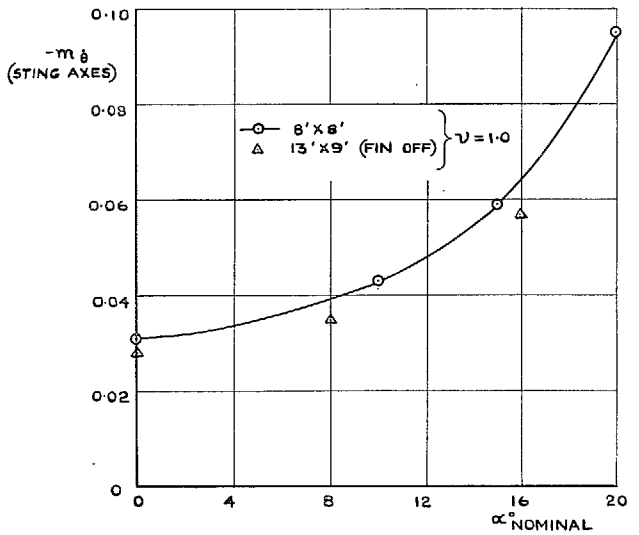

FIG. 10. Damping in pitch, $-m_{\dot{\theta}}$. Variation with incidence. $V = 200$ ft/sec.

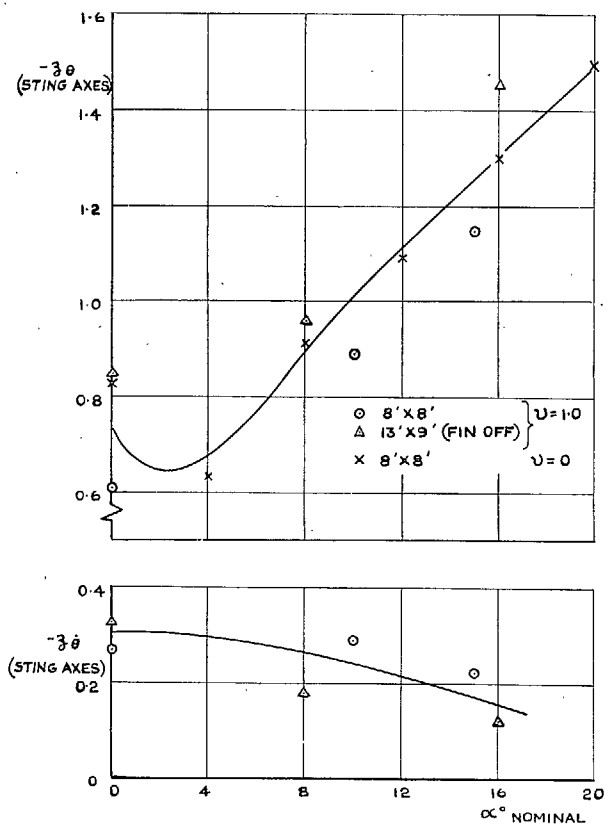

FIG. 11. Cross derivatives, $-z_\theta$ and $-z_{\dot{\theta}}$. Variation with incidence. $V = 200$ ft/sec.

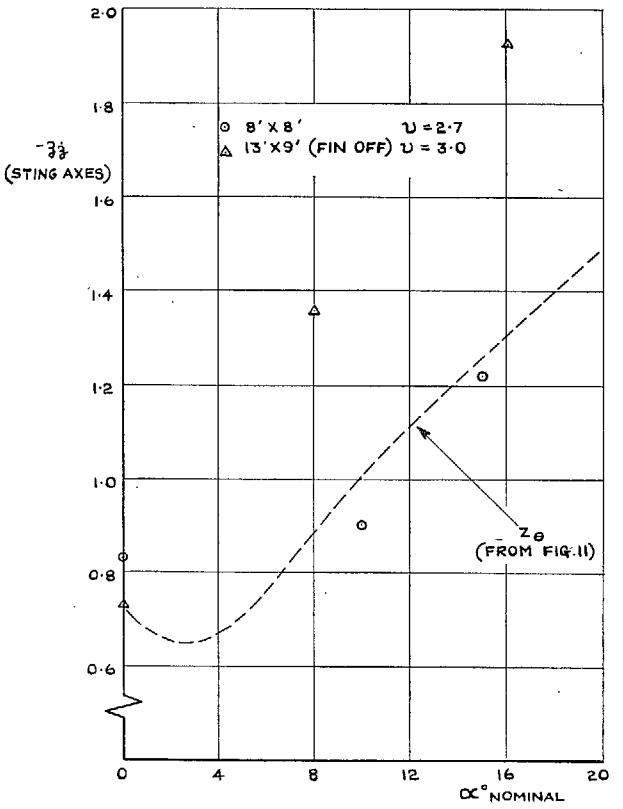

FIG. 12. Damping in heave, $-z_{\dot{z}}$. Variation with incidence. $V = 200$ ft/sec.

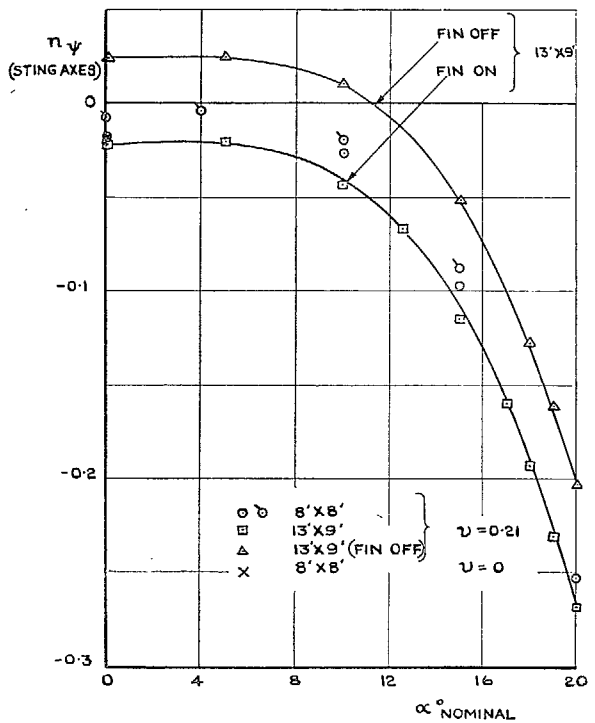

FIG. 13. Stability in yaw, n_ψ. Variation with incidence. $V = 200$ ft/sec.

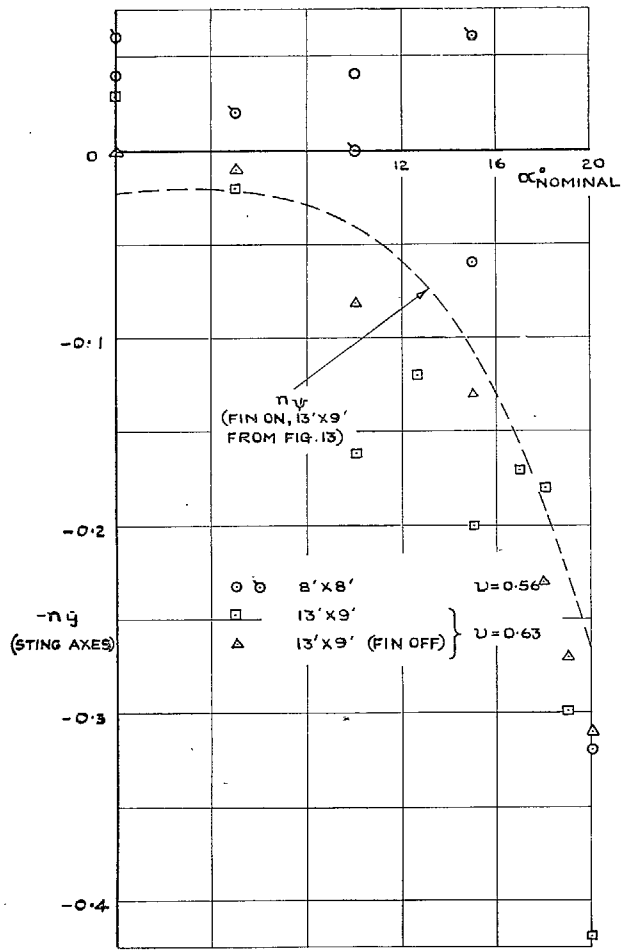

FIG. 14. Stability in yaw, $-n_{\dot{y}}$. Variation with incidence. $V = 200$ ft/sec.

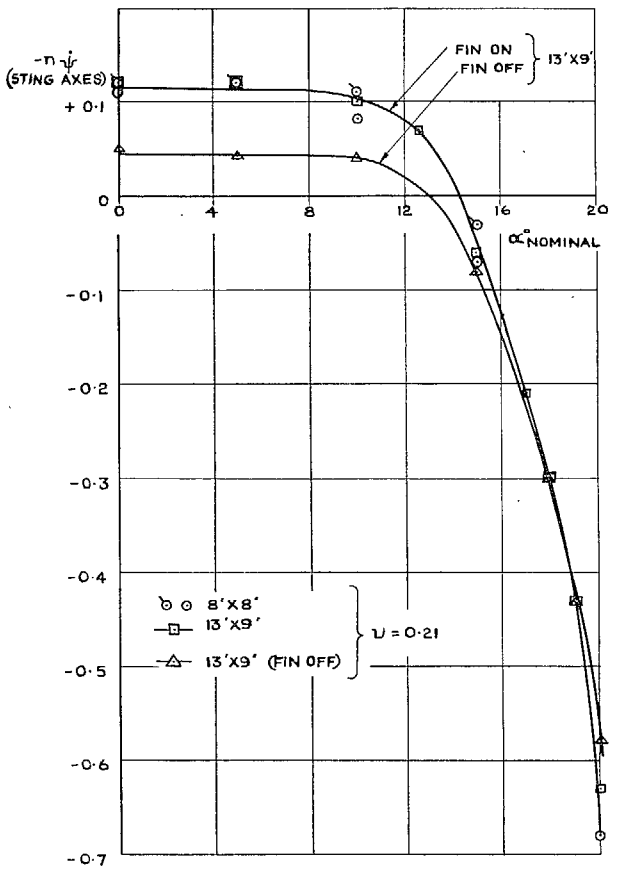

FIG. 15. Damping in yaw, $-n_{\dot{\psi}}$. Variation with incidence. $V = 200$ ft/sec.

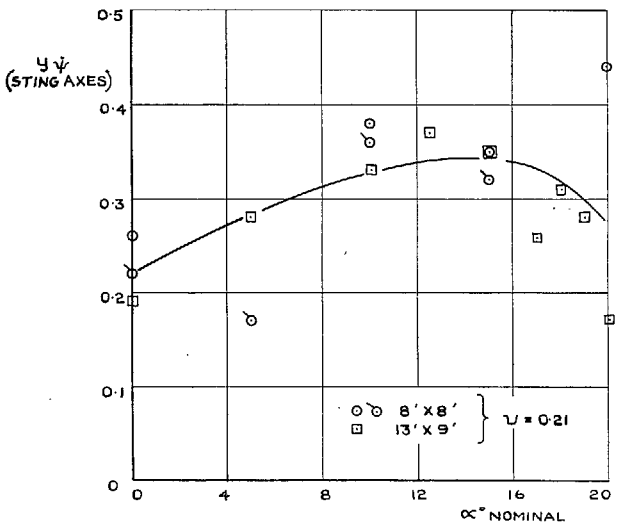

FIG. 16. Cross derivative, $y_{\dot{\psi}}$. Variation with incidence. $V = 200$ ft/sec.

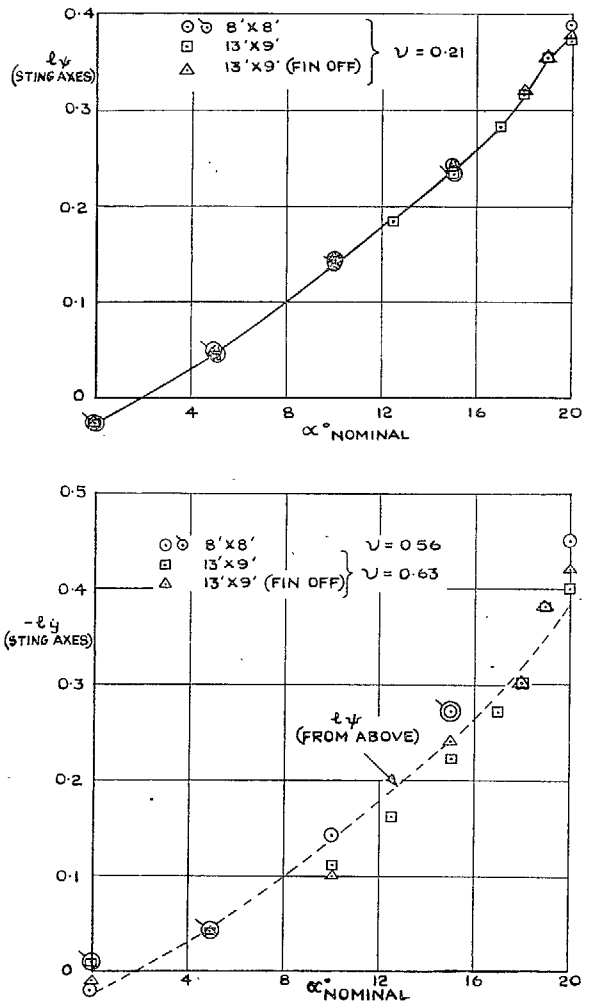

FIG. 17. Cross derivatives, l_ψ and $-l_{\dot{y}}$. Variation with incidence. $V = 200$ ft/sec.

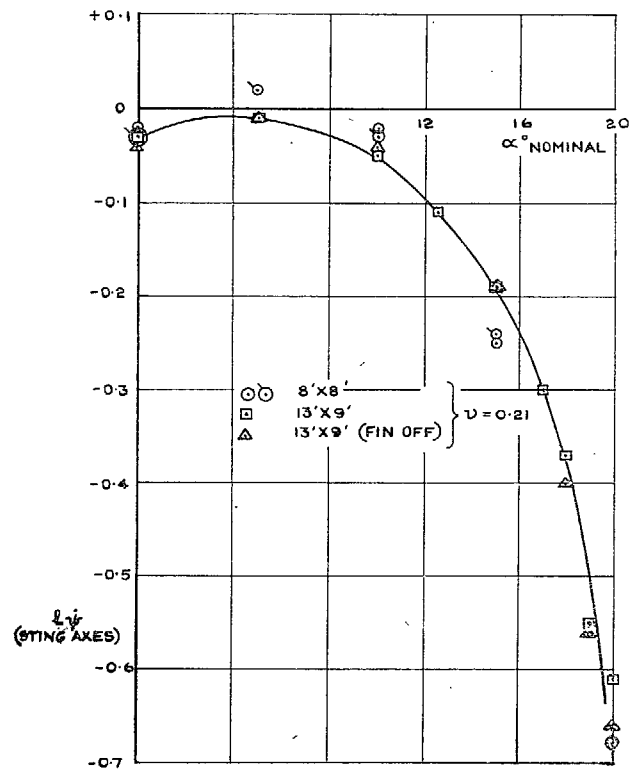

FIG. 18. Cross derivative, $l_{\dot{\psi}}$. Variation with incidence. $V = 200$ ft/sec.

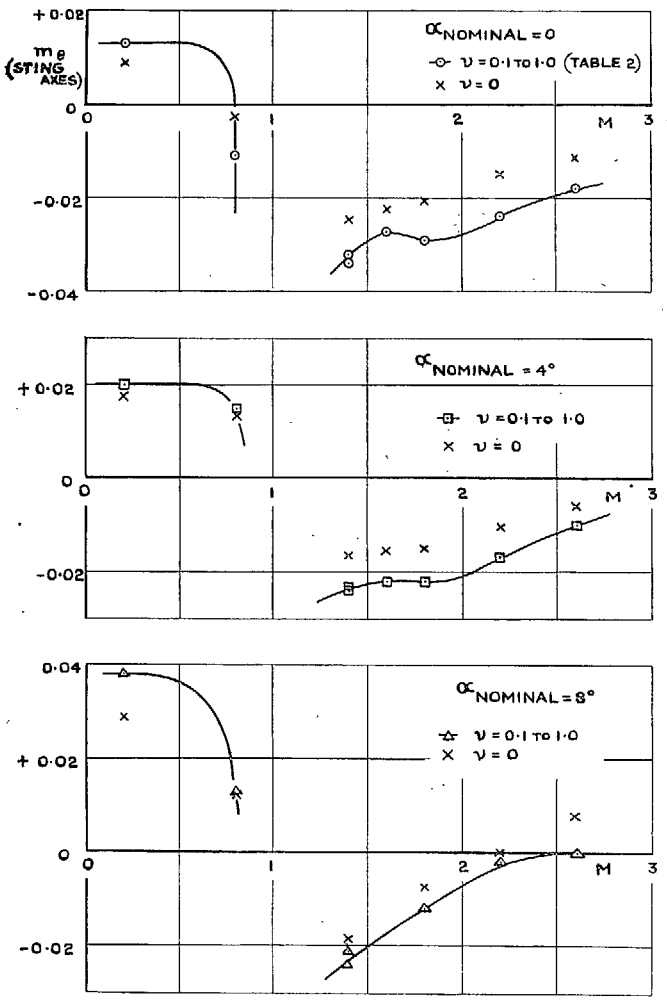

FIG. 19. Stability in pitch, m_θ. Variation with Mach number.

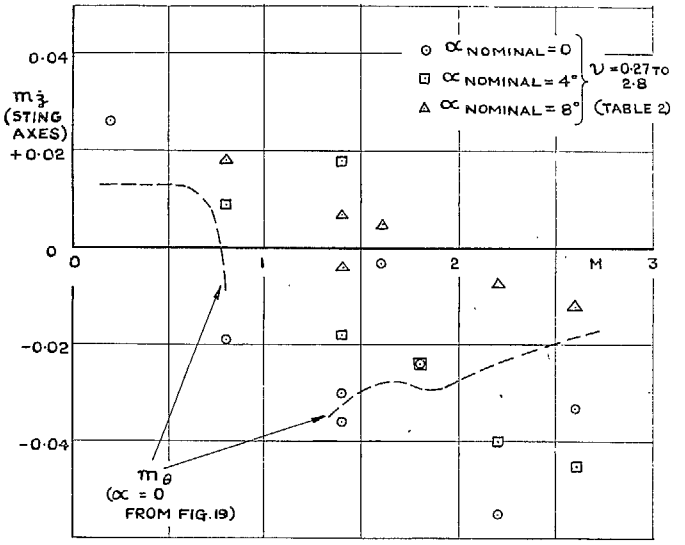

FIG. 20. Stability in pitch, $m_{\dot{z}}$. Variation with Mach number.

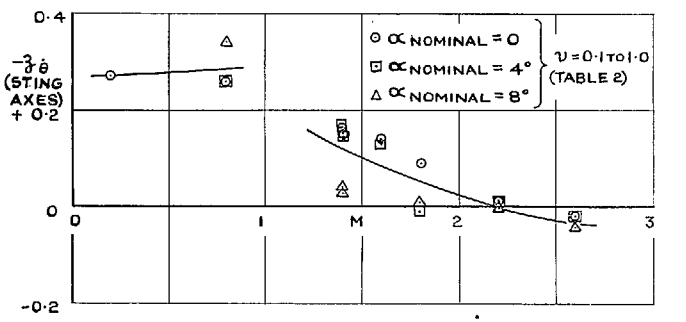

FIG. 21. Cross derivative, $-z_{\dot{\theta}}$. Variation with Mach number.

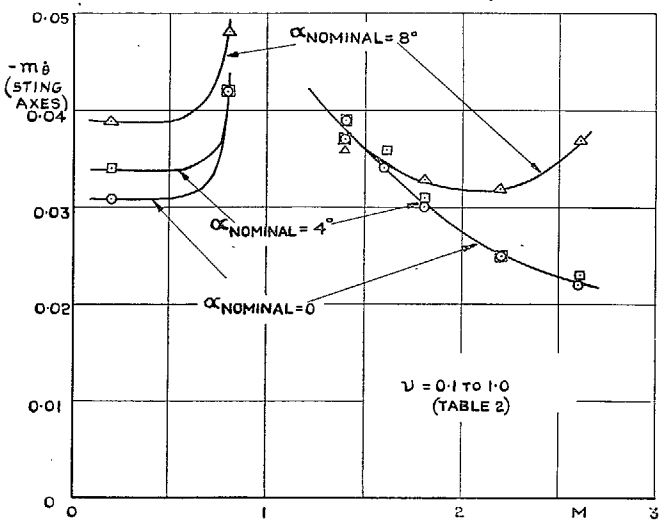

FIG. 22. Damping in pitch, $-m_{\dot{\theta}}$. Variation with Mach number.

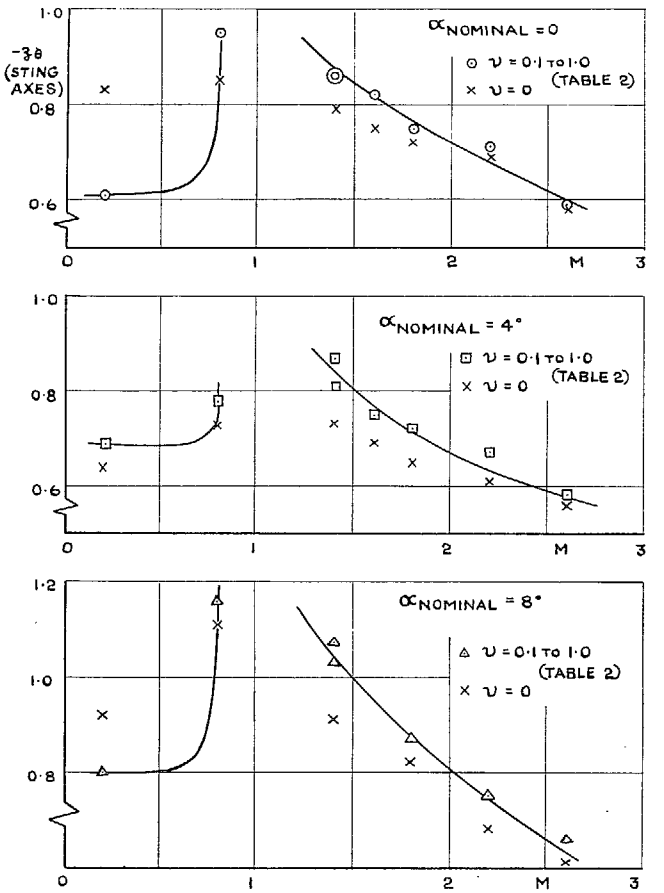

FIG. 23. Cross derivative, $-z_{\dot{\theta}}$. Variation with Mach number.

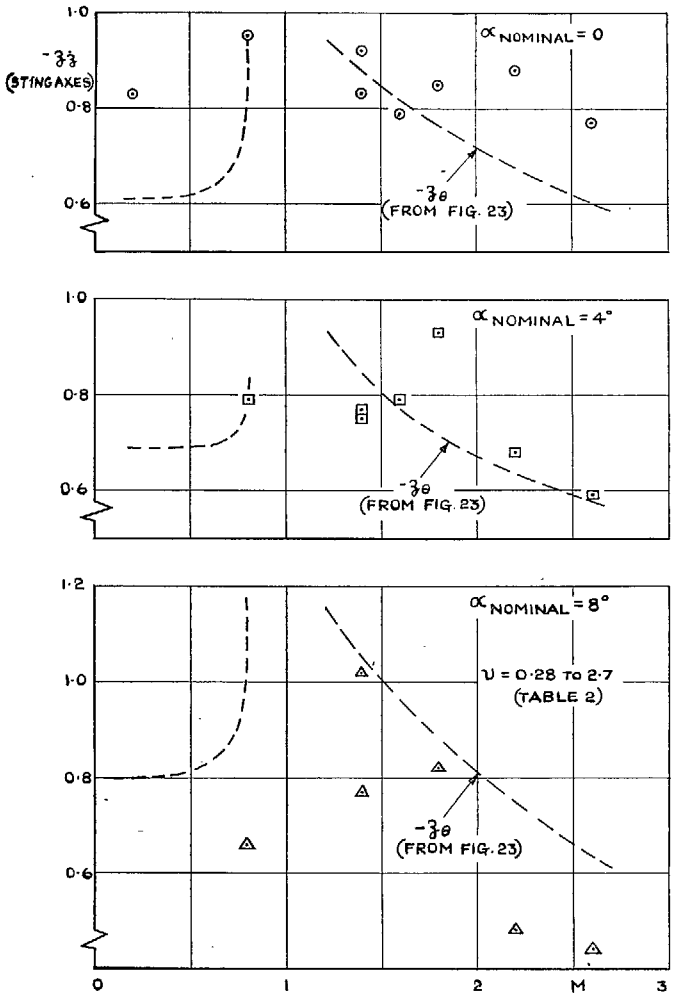

FIG. 24. Damping in heave, $-z_{\dot{z}}$. Variation with Mach number.

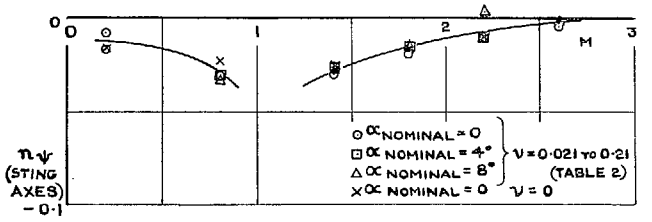

FIG. 25. Stability in yaw, n_ψ. Variation with Mach number.

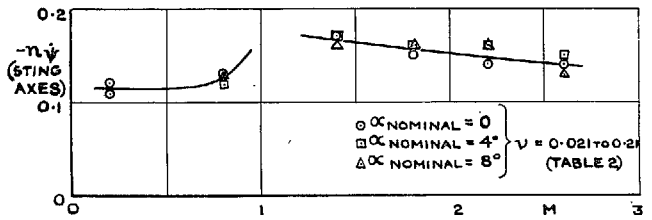

FIG. 26. Damping in yaw, $-n_{\dot{\psi}}$. Variation with Mach number.

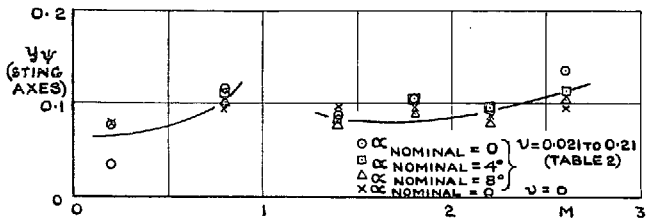

FIG. 27. Cross derivative, y_ψ. Variation with Mach number.

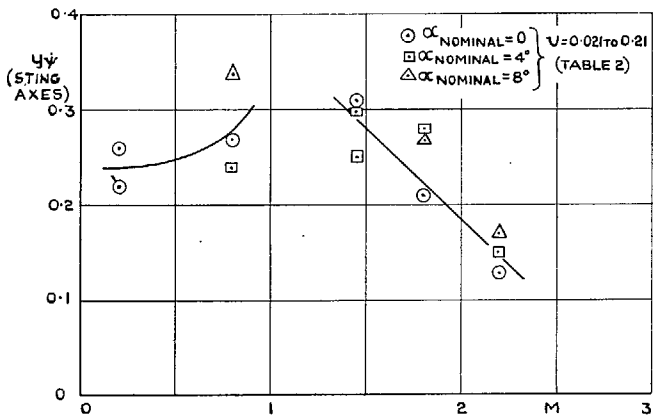

FIG. 28. Cross derivative, y_ψ. Variation with Mach number.

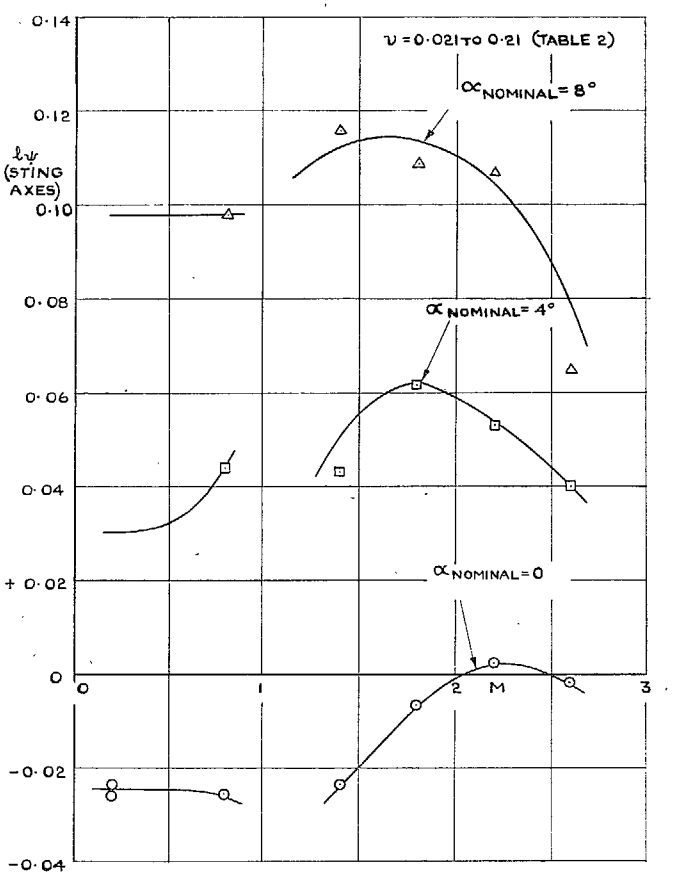

FIG. 29. Cross derivative, l_ψ. Variation with Mach number.

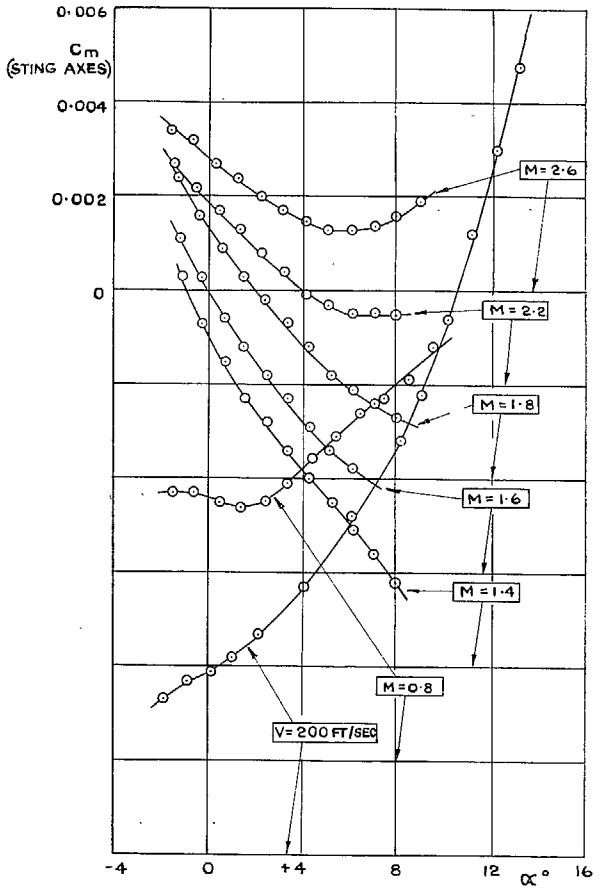

FIG. 30. Static pitching moment, C_m. Variation with incidence.

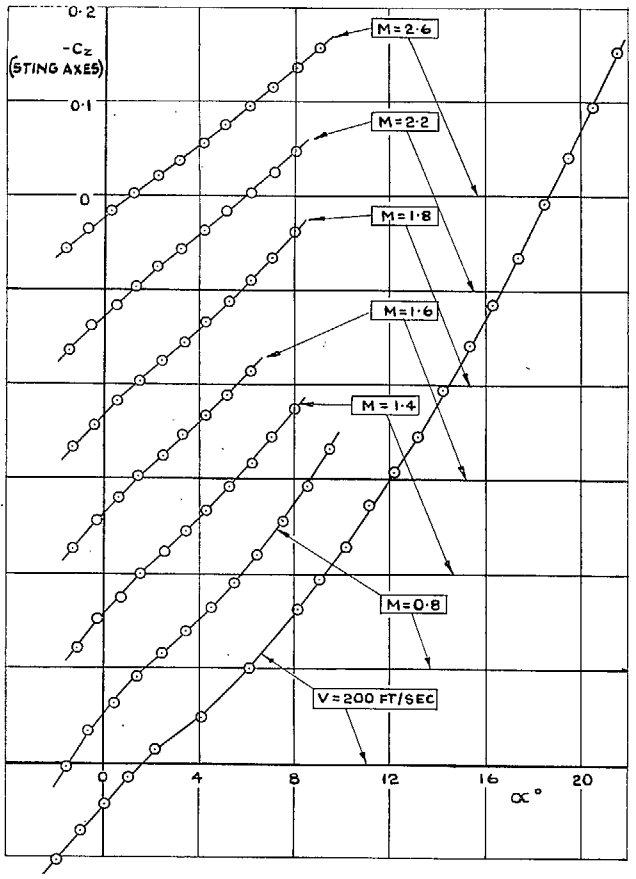

FIG. 31. Static normal force, $-C_z$. Variation with incidence.

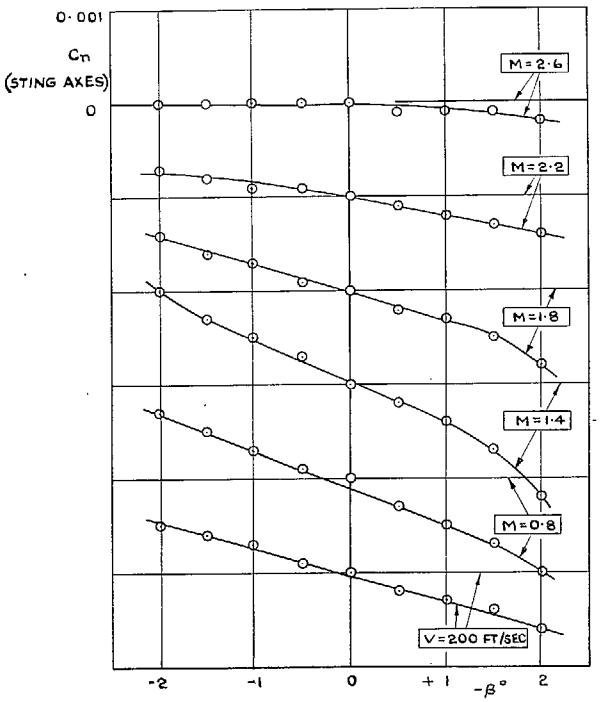

FIG. 32. Static yawing moment, C_n. Variation with sideslip. $\alpha = 0$.

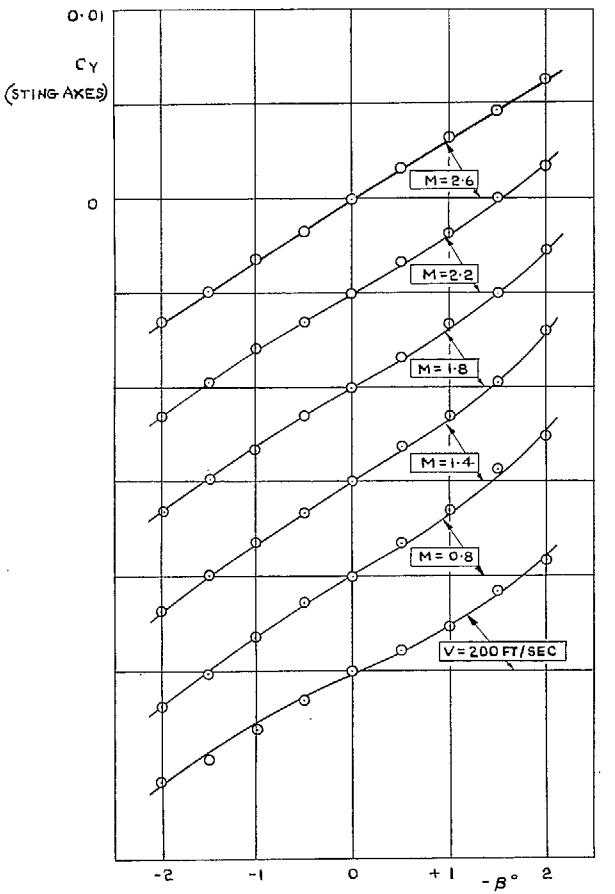

FIG. 33. Static side force, C_y. Variation with sideslip. $\alpha = 0$.

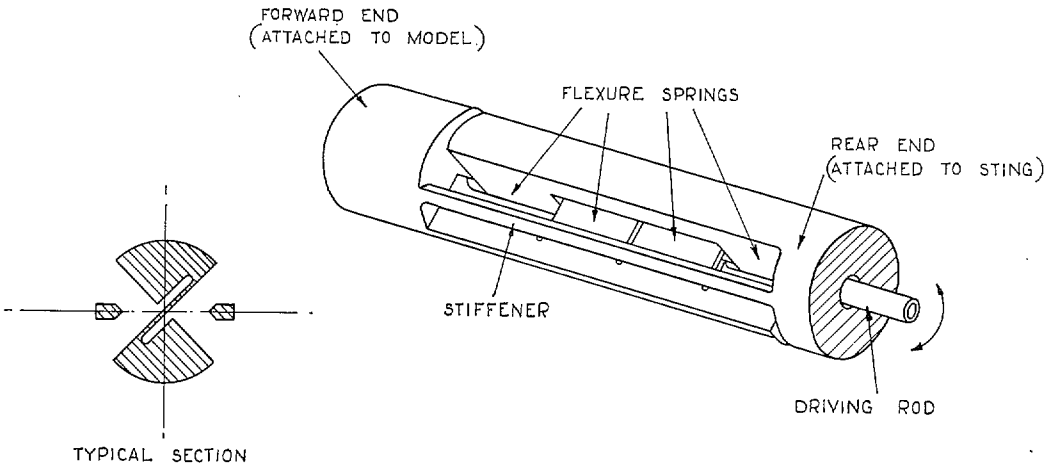

FIG. 34. Roll spring unit.

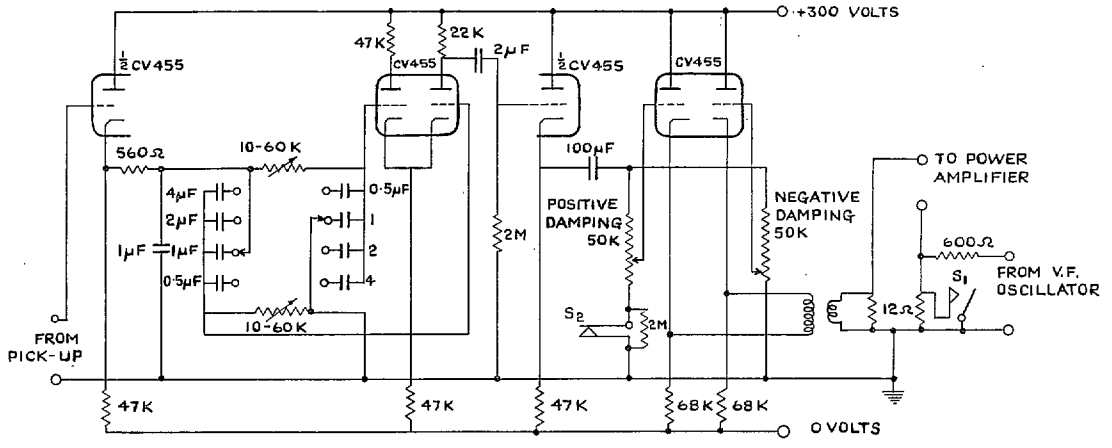

FIG. 35. Feedback amplifier.

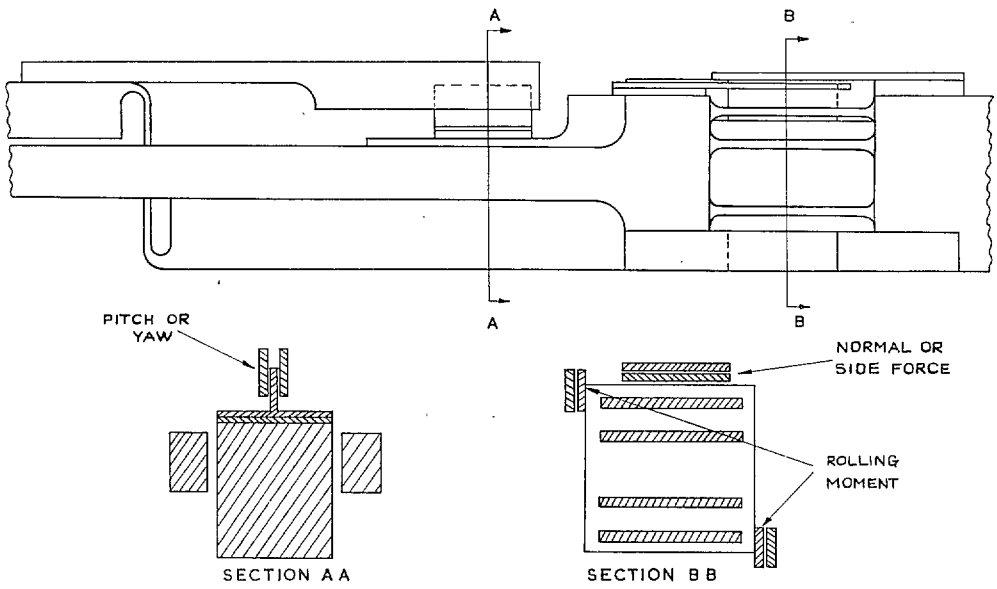

FIG. 36. Force and displacement pick-ups.

(88725) Wt. 65/1418 K.5 2/64 Hw.

Publications of the Aeronautical Research Council

ANNUAL TECHNICAL REPORTS OF THE AERONAUTICAL RESEARCH COUNCIL (BOUND VOLUMES)

1942 Vol. I. Aero and Hydrodynamics, Aerofoils, Airscrews, Engines. 75*s.* (post 2*s.* 9*d.*)
Vol. II. Noise, Parachutes, Stability and Control, Structures, Vibration, Wind Tunnels. 47*s.* 6*d.* (post 2*s.* 3*d.*)

1943 Vol. I. Aerodynamics, Aerofoils, Airscrews. 80*s.* (post 2*s.* 6*d.*)
Vol. II. Engines, Flutter, Materials, Parachutes, Performance, Stability and Control, Structures. 90*s.* (post 2*s.* 9*d.*)

1944 Vol. I. Aero and Hydrodynamics, Aerofoils, Aircraft, Airscrews, Controls. 84*s.* (post 3*s.*)
Vol. II. Flutter and Vibration, Materials, Miscellaneous, Navigation, Parachutes, Performance, Plates and Panels, Stability, Structures, Test Equipment, Wind Tunnels. 84*s.* (post 3*s.*)

1945 Vol. I. Aero and Hydrodynamics, Aerofoils. 130*s.* (post 3*s.* 6*d.*)
Vol. II. Aircraft, Airscrews, Controls. 130*s.* (post 3*s.* 6*d.*)
Vol. III. Flutter and Vibration, Instruments, Miscellaneous, Parachutes, Plates and Panels, Propulsion. 130*s.* (post 3*s.* 3*d.*)
Vol. IV. Stability, Structures, Wind Tunnels, Wind Tunnel Technique. 130*s.* (post 3*s.* 3*d.*)

1946 Vol. I. Accidents, Aerodynamics, Aerofoils and Hydrofoils. 168*s.* (post 3*s.* 9*d.*)
Vol. II. Airscrews, Cabin Cooling, Chemical Hazards, Controls, Flames, Flutter, Helicopters, Instruments and Instrumentation, Interference, Jets, Miscellaneous, Parachutes. 168*s.* (post 3*s.* 3*d.*)
Vol. III. Performance, Propulsion, Seaplanes, Stability, Structures, Wind Tunnels. 168*s.* (post 3*s.* 6*d.*)

1947 Vol. I. Aerodynamics, Aerofoils, Aircraft. 168*s.* (post 3*s.* 9*d.*)
Vol. II. Airscrews and Rotors, Controls, Flutter, Materials, Miscellaneous, Parachutes, Propulsion, Seaplanes, Stability, Structures, Take-off and Landing. 168*s.* (post 3*s.* 9*d.*)

1948 Vol. I. Aerodynamics, Aerofoils, Aircraft, Airscrews, Controls, Flutter and Vibration, Helicopters, Instruments, Propulsion, Seaplane, Stability, Structures, Wind Tunnels. 130*s.* (post 3*s.* 3*d.*)
Vol. II. Aerodynamics, Aerofoils, Aircraft, Airscrews, Controls, Flutter and Vibration, Helicopters, Instruments, Propulsion, Seaplane, Stability, Structures, Wind Tunnels. 110*s.* (post 3*s.* 3*d.*)

Special Volumes

Vol. I. Aero and Hydrodynamics, Aerofoils, Controls, Flutter, Kites, Parachutes, Performance, Propulsion, Stability. 126*s.* (post 3*s.*)
Vol. II. Aero and Hydrodynamics, Aerofoils, Airscrews, Controls, Flutter, Materials, Miscellaneous, Parachutes, Propulsion, Stability, Structures. 147*s.* (post 3*s.*)
Vol. III. Aero and Hydrodynamics, Aerofoils, Airscrews, Controls, Flutter, Kites, Miscellaneous, Parachutes, Propulsion, Seaplanes, Stability, Structures, Test Equipment. 189*s.* (post 3*s.* 9*d.*)

Reviews of the Aeronautical Research Council

1939–48 3*s.* (post 6*d.*) 1949–54 5*s.* (post 5*d.*)

Index to all Reports and Memoranda published in the Annual Technical Reports

1909–1947 R. & M. 2600 (out of print)

Indexes to the Reports and Memoranda of the Aeronautical Research Council

Between Nos. 2351–2449	R. & M. No. 2450 2*s.* (post 3*d.*)
Between Nos. 2451–2549	R. & M. No. 2550 2*s.* 6*d.* (post 3*d.*)
Between Nos. 2551–2649	R. & M. No. 2650 2*s.* 6*d.* (post 3*d.*)
Between Nos. 2651–2749	R. & M. No. 2750 2*s.* 6*d.* (post 3*d.*)
Between Nos. 2751–2849	R. & M. No. 2850 2*s.* 6*d.* (post 3*d.*)
Between Nos. 2851–2949	R. & M. No. 2950 3*s.* (post 3*d.*)
Between Nos. 2951–3049	R. & M. No. 3050 3*s.* 6*d.* (post 3*d.*)
Between Nos. 3051–3149	R. & M. No. 3150 3*s.* 6*d.* (post 3*d.*)

HER MAJESTY'S STATIONERY OFFICE

from the addresses overleaf

Printed and published by
HER MAJESTY'S STATIONERY OFFICE

To be purchased from
York House, Kingsway, London W.C.2
423 Oxford Street, London W.1
13A Castle Street, Edinburgh 2
109 St. Mary Street, Cardiff
39 King Street, Manchester 2
50 Fairfax Street, Bristol 1
35 Smallbrook, Ringway, Birmingham 5
80 Chichester Street, Belfast 1
or through any bookseller

Printed in England

S.O. Code No. 23-3355